npj | digital medicine

Article

Published in partnership with Seoul National University Bundang Hospital

https://doi.org/10.1038/s41746-025-02250-5

Multi-step retrieval and reasoning improves radiology question answering with large language models

Check for updates

Sebastian Wind[1,2], Jeta Sopa[1], Daniel Truhn[3], Mahshad Lotfinia[3], Tri-Thien Nguyen[1,4], Keno Bressem[5,6], Lisa Adams[6], Mirabela Rusu[7,8], Harald Köstler[2,9], Gerhard Wellein[2], Andreas Maier[1,2] & Soroosh Tayebi Arasteh[1,3,7,8] ✉

Large language models (LLMs) show promise for radiology decision support, yet conventional retrieval-augmented generation (RAG) relies on single-step retrieval and struggles with complex reasoning. We introduce radiology Retrieval and Reasoning (RaR), a multi-step retrieval framework that iteratively summarizes clinical questions, retrieves evidence, and synthesizes answers. We evaluated 25 LLMs spanning general-purpose, reasoning-optimized, and clinically fine-tuned models (0.5B → 670B parameters) on 104 expert-curated radiology questions and an independent set of 65 real radiology board-exam questions. RaR significantly improved mean diagnostic accuracy versus zero-shot prompting (75% vs. 67%; $P = 1.1 \times 10^{-7}$) and conventional online RAG (75% vs. 69%; $P = 1.9 \times 10^{-6}$). Gains were largest in mid-sized and small models (e.g., Mistral Large: 72% → 81%), while very large models showed minimal change. RaR reduced hallucinations and provided clinically relevant evidence in 46% of cases, improving factual grounding. These results show that multi-step retrieval enhances diagnostic reliability, especially in deployable mid-sized LLMs. Code, datasets, and RaR are publicly available.

Artificial intelligence (AI) is rapidly transforming diagnostic radiology by enhancing imaging interpretation, improving diagnostic precision, and streamlining clinical workflows[1,2]. Recent advances in large language models (LLMs)[3–7], such as GPT-4[8], have shown remarkable capability in extracting structured information from radiology reports, supporting clinical reasoning, and enabling natural language interfaces[3,9–12]. However, a key limitation persists: the static nature of LLM training data, which may lead to incomplete, outdated, or biased knowledge, thereby compromising clinical accuracy and reliability.

Retrieval-augmented generation (RAG)[13], first introduced by Lewis et al., predates modern large language models and broadly combines generative models with external corpora to ground outputs in retrieved information. When paired with domain-specific knowledge sources, RAG can improve factual accuracy and reduce hallucinations[6,14–17], but its effectiveness depends critically on the quality and coverage of retrieval, and retrieved content is not guaranteed to be correct. Tayebi Arasteh et al. recently introduced Radiology RAG (RadioRAG)[18], an online RAG framework leveraging real-time content from Radiopaedia[19], which demonstrated substantial accuracy improvements in certain LLMs such as GPT-3.5-turbo compared to conventional zero-shot inference. However, these gains were inconsistent, with models like Llama3-8B showing negligible improvements, reflecting limitations in traditional single-step retrieval architectures. Current online RAG frameworks[16,18,20], including RadioRAG[18], primarily employ a single-step retrieval and generation process, limiting their ability to manage complex, multi-part clinical questions[21]. These designs lack iterative refinement, dynamic query expansion, and systematic evaluation of intermediate uncertainty[20]. To address these gaps, multi-step retrieval and reasoning frameworks have

[1]Pattern Recognition Lab, Friedrich-Alexander-Universität Erlangen-Nürnberg, Erlangen, Germany. [2]Erlangen National High Performance Computing Center, Friedrich-Alexander-Universität Erlangen-Nürnberg, Erlangen, Germany. [3]Department of Diagnostic and Interventional Radiology, University Hospital RWTH Aachen, Aachen, Germany. [4]Institute of Radiology, University Hospital Erlangen, Erlangen, Germany. [5]Department of Cardiovascular Radiology and Nuclear Medicine, TUM University Clinic, School of medicine and Health, German Heart Center, Technical University of Munich, Munich, Germany. [6]Department of Diagnostic and Interventional Radiology, TUM University Clinic, School of Medicine and Health, Klinikum rechts der Isar, Technical University of Munich, Munich, Germany. [7]Department of Radiology, Stanford University, Stanford, CA, USA. [8]Department of Urology, Stanford University, Stanford, CA, USA. [9]Chair of Computer Science 10, Friedrich-Alexander-Universität Erlangen-Nürnberg, Erlangen, Germany. ✉e-mail: soroosh.arasteh@rwth-aachen.de

recently emerged as an advanced paradigm in AI research[3,22–24]. Recent work in medicine, including i-MedRAG[25], MedAide[26], MedAgentBench[27], and MedChain[28], and more specifically recent works in radiology such as CT-Agent[29] for computed tomography QA, RadCouncil[30] and Yi et al.[31] for report generation, and agent-based uncertainty awareness for report labeling[32] further underscores their growing role in improving factual reliability and interpretability. Such approaches enable LLMs to orchestrate retrieval[33], reasoning, and synthesis in iterative multi-step chains[34,35], supporting dynamic adaptation and enhanced problem-solving capabilities[36–38]. They have shown success across domains such as oncology, general clinical decision-making, and biomedical research[22,23,39], improving both accuracy and interpretability compared to static prompting and conventional RAG. Despite these promising outcomes, their utility in radiology remains largely unexplored, even though radiology uniquely demands nuanced, multi-step reasoning and retrieval of specialized domain knowledge[40].

In this study, we address this crucial gap by systematically evaluating the effectiveness of multi-step retrieval and reasoning in text-based radiology question answering (QA). We introduce radiology Retrieval and Reasoning (RaR), a framework that decomposes clinical questions into structured diagnostic options, retrieves targeted evidence from the comprehensive, peer-reviewed Radiopaedia.org knowledge base, and synthesizes evidence-based responses through iterative reasoning. Using 104 expert-curated radiology questions from the RSNA-RadioQA and ExtendedQA datasets of the RadioRAG study[18] (see Supplementary Table 1 for dataset characteristics), we compare zero-shot inference, conventional online RAG, and RaR. To assess generalizability, we additionally evaluate RaR on an independent internal dataset of 65 authentic board-style radiology questions from the Technical University of Munich, reflecting real-world assessment conditions and minimizing risk of data leakage. Across 25 diverse LLMs—including proprietary systems (GPT-4-turbo[8], GPT-5, o3), open-weight models (Mistral Large, Qwen 2.5[41]), and clinically fine-tuned variants (MedGemma[42], Llama3-Med42[43])—spanning small (0.5B) to mid-sized (17–110B) and very large architectures (>200B, e.g., DeepSeek-R1[44], o3), we systematically assess the impact of retrieval and reasoning on radiology QA (see Table 1). Our results show that RaR consistently enhances diagnostic accuracy and factual reliability across most model classes, with the largest gains in small and mid-sized models where conventional retrieval is insufficient. Very large models (>200B) with strong internal reasoning benefit less, likely due to extensive pretraining and generalization ability, yet even clinically fine-tuned models demonstrate meaningful improvements, suggesting that retrieval and fine-tuning offer complementary strengths. RaR also reduces hallucinations and surfaces clinically relevant content that assists not only LLMs but also radiologists, underscoring its potential to improve factuality, accuracy, and interpretability. Figure 1 provides an overview of the pipeline, and Fig. 2 illustrates a representative worked example, with additional methodological details in Materials and Methods. Importantly, this study focuses on text-only radiology QA, and future work should extend RaR to multimodal tasks involving imaging data.

Results

Comparison of zero-shot, conventional RAG, and RaR across models

We assessed the diagnostic performance of 25 LLMs across three distinct inference strategies: zero-shot prompting, conventional online RAG, and our proposed RaR framework. The LLMs included: Ministral-8B, Mistral Large, Llama3.3-8B[45,46], Llama3.3-70B[45,46], Llama3-Med42-8B[43], Llama3-Med42-70B[43], Llama4 Scout 16E[33], DeepSeek R1-70B[44], DeepSeek-R1[44], DeepSeek-V3[47], Qwen 2.5-0.5B[41], Qwen 2.5-3B[41], Qwen 2.5-7B[41], Qwen 2.5-14B[41], Qwen 2.5-70B[41], Qwen 3-8B[48], Qwen 3-235B[48], GPT-3.5-turbo, GPT-4-turbo[8], o3, GPT-5[49], MedGemma-4B-it[42], MedGemma-27B-text-it[42], Gemma-3-4B-it[50,51], and Gemma-3-27B-it[50,51]. Accuracy was measured using the 104-question RadioRAG benchmark dataset, with detailed results presented in Table 2. When aggregating results across all LLMs, RaR demonstrated a statistically significant improvement in accuracy compared to zero-shot prompting ($P = 1.1 \times 10^{-7}$). As previously established, the traditional RAG approach also outperformed zero-shot prompting, showing a smaller but statistically significant gain ($P = 0.019$). Importantly, RaR further outperformed traditional online RAG ($P = 1.9 \times 10^{-6}$), underscoring the benefit of iterative retrieval and autonomous reasoning over single-pass retrieval pipelines. These findings indicate that, at the group level, RaR introduces measurable and additive improvements in radiology question answering, even when compared against established, high-performing RAG systems. The retrieval stage of RaR was guided by a diagnostic abstraction step that condensed each question into key clinical concepts to enable focused evidence search (see Supplementary Note 1 for examples and implementation details).

Factual consistency and hallucination rates

To assess factual reliability under RaR, we conducted a hallucination analysis across all 25 LLMs using the 104-question RadioRAG benchmark. Each response was reviewed by a board-certified radiologist (T.T.N.) to evaluate (i) whether the retrieved context was clinically relevant, (ii) whether the model's answer was grounded in that context, and (iii) whether the final output was factually correct. Context was classified as relevant only if it contained no incorrect or off-topic content relative to the diagnostic question, a deliberately strict criterion. Under this definition, clinically relevant evidence was retrieved in 46% of cases (48/104). Detailed results are provided in Table 3. To test whether RaR's gains depended on retrieval quality, we repeated the analysis using only the 48 questions with clinically relevant retrieved context. On this subset, RaR significantly improved accuracy across models (68% → 81%; $P = 5.1 \times 10^{-9}$; Supplementary Table 2), indicating that its benefits persist even under fully correct retrieval. Across the full dataset (104 questions), RaR increased mean accuracy from 67% → 75%. This comparison shows that RaR yields its largest improvements when accurate evidence is available (+13 vs. +8 percentage points overall) while remaining robust to retrieval noise.

When relevant context was available, most models demonstrated strong factual alignment. Hallucinations, defined as incorrect answers despite the presence of relevant context, occurred in only 9.4% ± 5.9 of questions. The lowest hallucination rates were observed in large-scale and reasoning-optimized models such as o3 (2%), DeepSeek-R1 (3%), and GPT-5 (3%), reflecting their superior ability to integrate and interpret retrieved content (see Fig. 3). In contrast, smaller models such as Qwen 2.5-0.5B (26%) and Gemma-3-4B-it (20%) struggled to do so reliably, exhibiting significantly higher rates of unsupported reasoning.

Interestingly, a substantial proportion of RaR responses were correct despite the retrieved context being clinically irrelevant. On average, 37.4% ± 4.9 of responses fell into this category. This behavior was particularly pronounced among models with strong internal reasoning capabilities, DeepSeek-V3, o3, and Qwen 3-235B each exceeded 40%, suggesting that in the absence of relevant evidence, these models often defaulted to internal knowledge. Similar trends were observed in mid-sized and clinically aligned models, such as Llama3.3-70B, Mistral Large, and MedGemma-27B-text-it, which also maintained high accuracy without external grounding. Conversely, smaller models like Qwen 2.5-0.5B (21%) and Ministral-8B (35%) were less effective under these conditions, indicating greater dependence on successful retrieval.

Across models, an average of 14.3% ± 6.5 of questions were answered incorrectly under zero-shot prompting but correctly after RaR, highlighting the additive diagnostic value of structured evidence acquisition. Supplementary Tables 3 and 4 provide example responses from GPT-3.5-turbo with and without RaR, alongside the corresponding retrieved content. These findings indicate that RaR improves factual grounding and reduces hallucination by enabling structured, clinically aware evidence refinement. However, model behavior in the absence of relevant context varies substantially, with larger and reasoning-tuned models demonstrating greater resilience through fallback internal reasoning. Representative examples of such cases, including model outputs that were correct despite irrelevant or noisy retrieval, are provided in Supplementary Note 2.

Table 1 | Specifications of the language models evaluated in this study

Model name	Parameters (billion)	Category	Accessibility	Knowledge cutoff date	Developer	Context length (thousand tokens)
Ministral-8B	8	IT	Open-source	October 2023	Mistral AI	128
Mistral Large	123	IT	Open-source	November 2024	Mistral AI	128
Llama3.3-8B	8	IT	Open-weights	March 2023	Meta AI	8
Llama3.3-70B	70	IT	Open-weights	December 2023	Meta AI	128
Llama3-Med42-8B	8	IT, clinically-aligned	Open-weights	August 2024	M42 Health AI Team	8
Llama3-Med42-70B	70	IT, clinically-aligned	Open-weights	August 2024	M42 Health AI Team	8
Llama4 Scout 16E	17	IT, 17B active parameters	Open-weights	August 2023	Meta AI	10,000 (10 M tokens)
DeepSeek R1-70B	70	Reasoning	Open-source	January 2025	DeepSeek	128
DeepSeek-R1	671	Reasoning	Open-source	January 2025	DeepSeek	128
DeepSeek-V3	671	Mixture of experts	Open-source	July 2024	DeepSeek	128
Qwen 2.5-0.5B	0.5	IT	Open-source	September 2024	Alibaba Cloud	32
Qwen 2.5-3B	3	IT	Open-source	September 2024	Alibaba Cloud	32
Qwen 2.5-7B	7	IT	Open-source	September 2024	Alibaba Cloud	131
Qwen 2.5-14B	14	IT	Open-source	September 2024	Alibaba Cloud	131
Qwen 2.5-70B	70	IT	Open-source	September 2024	Alibaba Cloud	131
Qwen 3-8B	8	Reasoning, mixture of experts	Open-source	December2024	Alibaba Cloud	32
Qwen 3-235B	235	Reasoning, mixture of experts	Open-source	July 2025	Alibaba Cloud	32
GPT-3.5-turbo	Undisclosed	IT	Proprietary	September 2021	OpenAI	16
GPT-4-turbo	Undisclosed	IT	Proprietary	December 2023	OpenAI	128
o3	Undisclosed	Reasoning	Proprietary	June 2024	OpenAI	200
GPT-5	Undisclosed	IT, reasoning	Proprietary	September 2024	OpenAI	128
MedGemma-4B-it	4	Gemma 3-based, multimodal, IT, clinical reasoning	Open-weights	July 2025	Google DeepMind	128
MedGemma-27B-text-it	27	Gemma 3-based, text only, IT, clinical reasoning	Open-weights	July 2025	Google DeepMind	≥ 128
Gemma-3-4B-it	4	IT	Open-weights	August 2024	Google DeepMind	128
Gemma-3-27B-it	27	IT	Open-weights	August 2024	Google DeepMind	128

Summary of the 25 LLMs assessed across zero-shot prompting, conventional online RAG, and the proposed radiology Retrieval and Reasoning (RaR). Listed for each model are parameter count (in billions), training category (e.g., instruction-tuned (IT), reasoning-optimized), accessibility, knowledge cutoff date, developer, and context length (in thousand tokens). Evaluations were conducted between July 1 and August 22, 2025. GPT-5 is included as a widely used system-level benchmark rather than a single fixed model architecture, as it dynamically routes queries across underlying models depending on the task.

To better understand the sources of model errors, we performed a qualitative error analysis across representative cases (see Supplementary Note 3). Three dominant error types were identified: reasoning shortcut errors, where models relied on familiar diagnostic patterns instead of verifying the retrieved evidence; context integration errors, where models correctly interpreted individual findings but failed to synthesize them into a coherent diagnosis; and context independence errors, where models produced correct answers despite disregarding the evidence. Overall, RaR markedly reduced shortcut and integration errors by promoting explicit evidence verification and contextual reasoning, correcting approximately 14.3% of previously wrong zero-shot answers.

Retrieval performance stratified by model scale: small-scale models

We next assessed whether model size influences the effectiveness of RaR in radiology question answering (see Fig. 4). Across the seven smallest models in our study (including Ministral-8B, Gemma-3-4B-it, Qwen 2.5-7B, Qwen 2.5-3B, Qwen 2.5-0.5B, Qwen 3-8B, and Llama-3-8B), we observed a consistent trend: conventional online RAG outperformed zero-shot prompting ($P = 0.002$), and RaR further improved over both baselines ($P = 0.016$ vs. zero-shot; $P = 0.035$ vs. traditional online RAG). When examining individual models, only two of the seven demonstrated statistically significant improvements with RaR compared to zero-shot prompting: Qwen 2.5-7B (71% ± 4 [95% CI: 62, 80] vs. 55% ± 5 [95% CI: 45, 64]; $P = 0.041$) and Ministral-8B (66% ± 5 [95% CI: 57, 76] vs. 47% ± 5 [95% CI: 38, 57]; $P = 0.020$). The remaining models exhibited absolute accuracy improvements ranging from 3 to 16%, though these did not reach statistical significance after correction for multiple comparisons.

These findings suggest that RaR can enhance performance in small-scale LLMs. However, the degree of benefit varied across models, likely reflecting differences in pretraining data, instruction tuning, and architectural design, even within a similar parameter range.

Retrieval performance stratified by model scale: large-scale models

We next evaluated the effect of RaR on the largest LLMs in our study, comprising DeepSeek-R1, DeepSeek-V3, o3, Qwen 3-235B, GPT-4-turbo, and GPT-5, all likely to be exceeding 200 billion parameters. These models demonstrated strong performance under zero-shot prompting alone, achieving diagnostic accuracies ranging from 76 to 86% on the RadioRAG

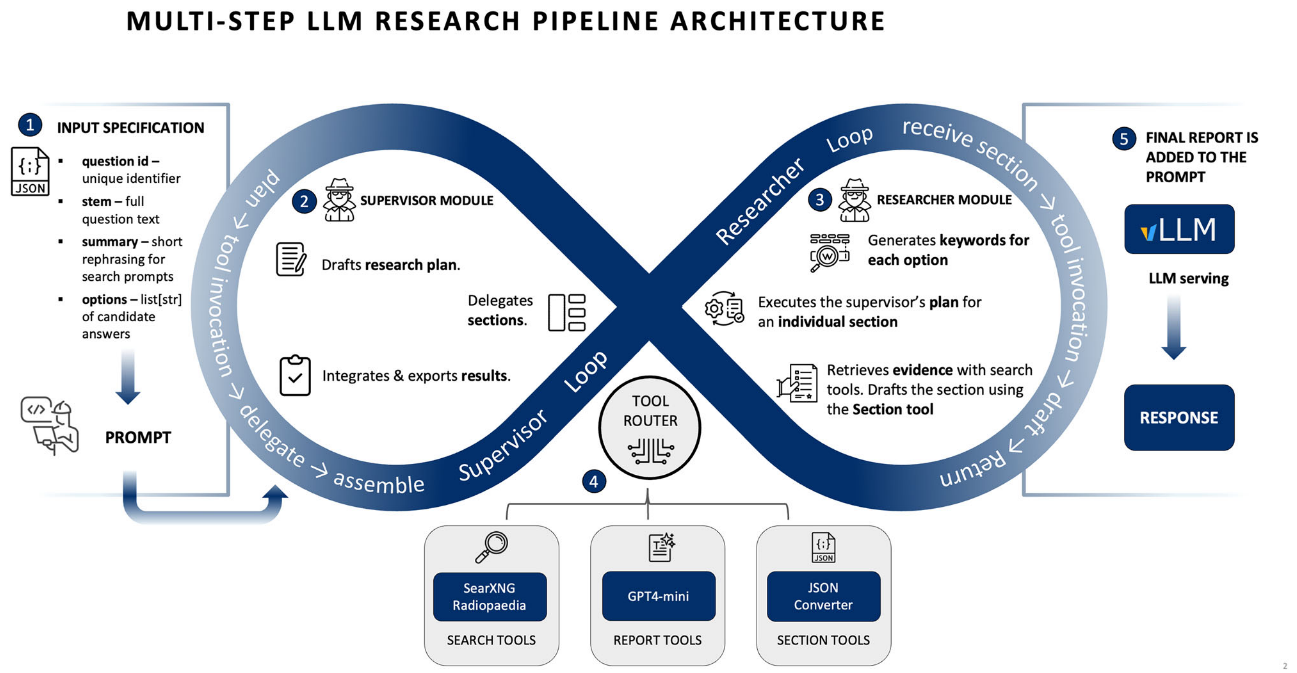
MULTI-STEP LLM RESEARCH PIPELINE ARCHITECTURE
1 INPUT SPECIFICATION
JSON
question id – unique identifier
stem – full question text
summary – short rephrasing for search prompts
options – list[str] of candidate answers
PROMPT
plan → tool invocation → delegate → assemble
Supervisor Loop
2 SUPERVISOR MODULE
Drafts research plan.
Delegates sections.
Integrates & exports results.
Researcher Loop
receive section → tool invocation → draft → Return
3 RESEARCHER MODULE
Generates keywords for each option
Executes the supervisor's plan for an individual section
Retrieves evidence with search tools. Drafts the section using the Section tool
TOOL ROUTER
4
SearXNG Radiopaedia
SEARCH TOOLS
GPT4-mini
REPORT TOOLS
JSON Converter
SECTION TOOLS
5 FINAL REPORT IS ADDED TO THE PROMPT
vLLM
LLM serving
RESPONSE

Fig. 1 | Multi-step architecture of the radiology Retrieval and Reasoning (RaR) framework for radiology question answering. The pipeline combines structured retrieval with multi-step reasoning to generate evidence-grounded diagnostic reports. (1) Each question is preprocessed to extract key diagnostic concepts (using Mistral Large) and paired with multiple-choice options. (2) A supervisor module creates a structured research plan, delegating each diagnostic option to a dedicated research module. (3) Research modules iteratively retrieve targeted evidence from www.radiopaedia.org via a SearXNG-powered search tool, refining queries when needed. (4) Retrieved content is synthesized into structured report sections (using GPT-4o-mini and formatting tools), including supporting and contradicting evidence with citations. (5) The supervisor compiles all sections into a final diagnostic report (introduction, analysis, and conclusion), which is appended to the prompt for final answer selection. The entire workflow is coordinated through a stateful directed graph that preserves shared memory, retrieved context, and intermediate drafts.

benchmark (Table 2). Neither conventional online RAG ($P = 0.999$) nor RaR ($P = 0.147$) led to meaningful improvements.

Across all five models, accuracy differences between the three inference strategies were minimal (see Fig. 4). For example, DeepSeek-R1 performed at 82% ± 4 [95% CI: 74, 89] with zero-shot, 80% ± 4 [95% CI: 72, 88] with RaR, and 79% ± 4 [95% CI: 71, 87] with conventional online RAG; o3 improved marginally from 86% ± 4 [95% CI: 78, 92] to 88% ± 3 [95% CI: 81, 93] with RaR; and Qwen3-235B and GPT-4-turbo showed ≤1% changes across conditions. DeepSeek-V3 and GPT-5 showed slightly higher improvement (DeepSeek-V3: from 76% ± 4 [95% CI: 67, 84] to 86% ± 4 [95% CI: 78, 92]; GPT-5: from 82% ± 4 [95% CI: 74, 89] to 88% ± 3 [95% CI: 82, 94], respectively) but still not significant. Traditional RAG showed similarly negligible differences.

These findings indicate that very large LLMs can already handle complex radiology QA tasks with high accuracy without requiring external retrieval. This likely reflects their extensive pretraining on large-scale corpora, improved reasoning abilities, and domain-general coverage, diminishing the marginal value of either conventional RAG or RaR in high-performing settings.

Retrieval performance stratified by model scale: mid-sized models

Mid-sized models, typically ranging between 17B and 110B parameters, represent a particularly relevant category for clinical deployment, offering a favorable trade-off between performance and computational efficiency. This group in our study included GPT-3.5-turbo, Llama 3.3-70B, Mistral Large, Qwen 2.5-70B, Llama 4 Scout 16E, Gemma-3-27B-it, and DeepSeek-R1-70B. Across this cohort, the conventional online RAG framework did not yield a statistically significant improvement in accuracy over zero-shot prompting ($P = 0.253$). In contrast, RaR significantly outperformed both zero-shot ($P = 0.001$) and conventional online RAG ($P = 0.002$), suggesting that the benefits of RaR become more apparent in this model size range, where LLMs are strong enough to follow reasoning chains but may still benefit from structured multi-step guidance. While every model in this group showed an absolute improvement in diagnostic accuracy with RaR, for example, GPT-3.5-turbo improved from 57 to 68%, Llama 3.3-70B from 76% ± 4 [95% CI: 67, 84] to 83% ± 4 [95% CI: 75, 89], and Mistral Large from 72% ± 4 [95% CI: 63, 81] to 81% ± 4 [95% CI: 73, 88], none of these increases reached statistical significance when evaluated individually (see Fig. 4).

To further probe the relationship between model scale and accuracy, we conducted a targeted scaling experiment using the Qwen 2.5 model family, which spans a wide range of sizes (Qwen 2.5-70B, 14B, 7B, 3B, and 0.5B) while maintaining consistent architecture and training procedures. This allowed us to isolate the influence of model size from confounding variables such as instruction tuning or pretraining corpus. We computed Pearson correlation coefficients between model size and diagnostic accuracy for each inference strategy. All three methods including zero-shot ($r = 0.68$), conventional online RAG ($r = 0.81$), and RaR ($r = 0.61$) showed strong positive correlations with parameter count, reflecting the general performance advantage of larger models. However, as detailed in earlier findings, the relative benefit of retrieval strategies was not uniformly distributed: conventional RAG was most beneficial for small models, while RaR consistently enhanced performance in mid-sized models (see Fig. 4). These findings highlight the importance of aligning retrieval strategies with model capacity and deployment constraints.

Effect of clinical fine-tuning on retrieval-augmented performance

To examine whether domain-specific fine-tuning diminishes the utility of retrieval-based strategies, we evaluated four clinically optimized language models: MedGemma-27B-text-it, MedGemma-4B-it, Llama3-Med42-70B, and Llama3-Med42-8B. These models are specifically fine-tuned for biomedical or radiological applications, making them suitable test cases for

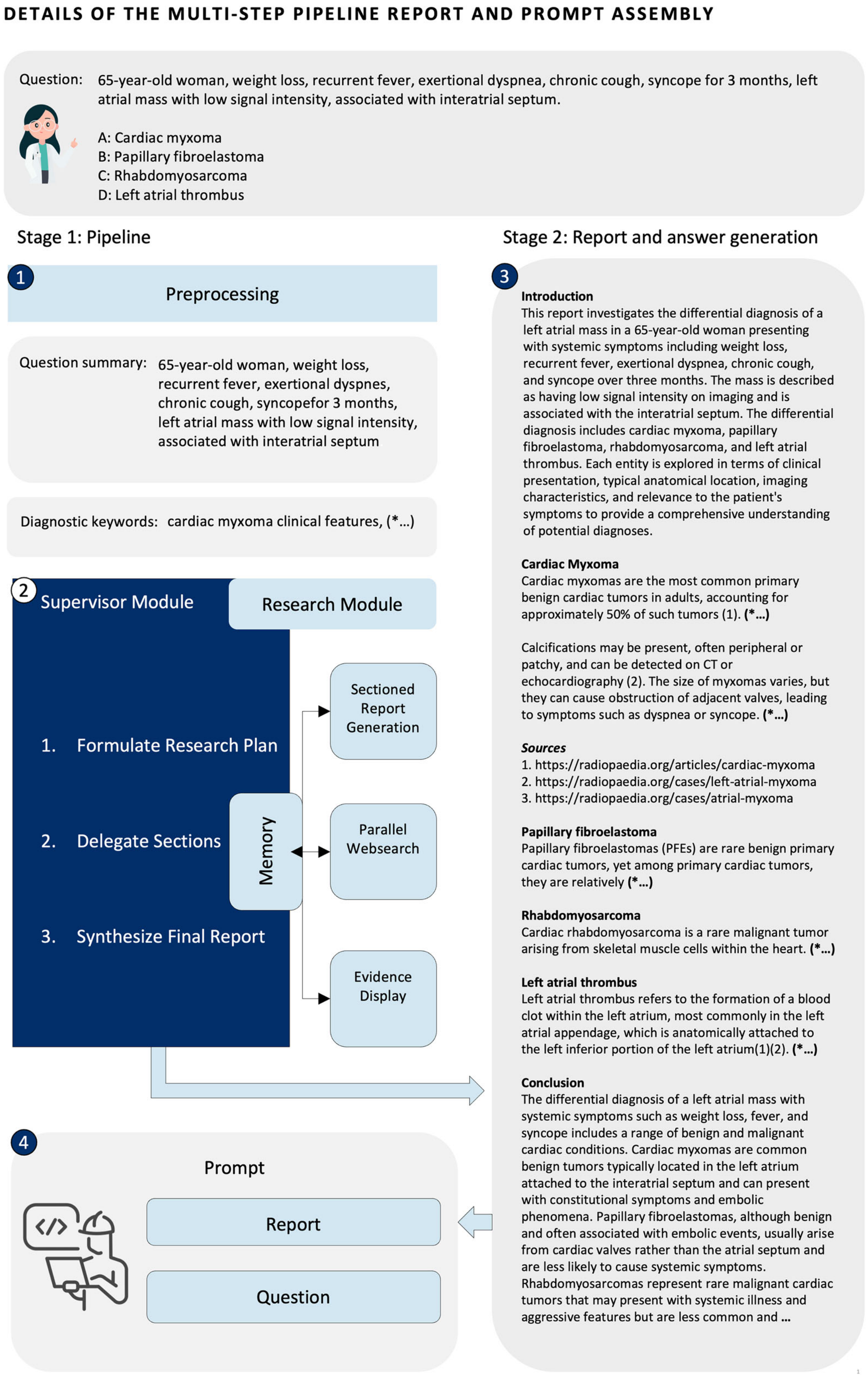

Question: 65-year-old woman, weight loss, recurrent fever, exertional dyspnea, chronic cough, syncope for 3 months, left atrial mass with low signal intensity, associated with interatrial septum.

A: Cardiac myxoma
B: Papillary fibroelastoma
C: Rhabdomyosarcoma
D: Left atrial thrombus

Question summary: 65-year-old woman, weight loss, recurrent fever, exertional dyspnes, chronic cough, syncopefor 3 months, left atrial mass with low signal intensity, associated with interatrial septum

Diagnostic keywords: cardiac myxoma clinical features, (*...)

Introduction
This report investigates the differential diagnosis of a left atrial mass in a 65-year-old woman presenting with systemic symptoms including weight loss, recurrent fever, exertional dyspnea, chronic cough, and syncope over three months. The mass is described as having low signal intensity on imaging and is associated with the interatrial septum. The differential diagnosis includes cardiac myxoma, papillary fibroelastoma, rhabdomyosarcoma, and left atrial thrombus. Each entity is explored in terms of clinical presentation, typical anatomical location, imaging characteristics, and relevance to the patient's symptoms to provide a comprehensive understanding of potential diagnoses.

Cardiac Myxoma
Cardiac myxomas are the most common primary benign cardiac tumors in adults, accounting for approximately 50% of such tumors (1). **(*...)**

Calcifications may be present, often peripheral or patchy, and can be detected on CT or echocardiography (2). The size of myxomas varies, but they can cause obstruction of adjacent valves, leading to symptoms such as dyspnea or syncope. **(*...)**

Sources
1. https://radiopaedia.org/articles/cardiac-myxoma
2. https://radiopaedia.org/cases/left-atrial-myxoma
3. https://radiopaedia.org/cases/atrial-myxoma

Papillary fibroelastoma
Papillary fibroelastomas (PFEs) are rare benign primary cardiac tumors, yet among primary cardiac tumors, they are relatively **(*...)**

Rhabdomyosarcoma
Cardiac rhabdomyosarcoma is a rare malignant tumor arising from skeletal muscle cells within the heart. **(*...)**

Left atrial thrombus
Left atrial thrombus refers to the formation of a blood clot within the left atrium, most commonly in the left atrial appendage, which is anatomically attached to the left inferior portion of the left atrium(1)(2). **(*...)**

Conclusion
The differential diagnosis of a left atrial mass with systemic symptoms such as weight loss, fever, and syncope includes a range of benign and malignant cardiac conditions. Cardiac myxomas are common benign tumors typically located in the left atrium attached to the interatrial septum and can present with constitutional symptoms and embolic phenomena. Papillary fibroelastomas, although benign and often associated with embolic events, usually arise from cardiac valves rather than the atrial septum and are less likely to cause systemic symptoms. Rhabdomyosarcomas represent rare malignant cardiac tumors that may present with systemic illness and aggressive features but are less common and ...

Fig. 2 | Representative example of the RaR process for a radiology question answering item. This figure shows the full RaR workflow for a representative question (RSNA-RadioQA-Q53) involving a patient with systemic symptoms and a low signal intensity left atrial mass associated with the interatrial septum. The pipeline begins with keyword-based summarization to guide retrieval, followed by parallel evidence searches for each diagnostic option using Radiopaedia.org. Retrieved content is synthesized into a structured report, including an introduction, citation-backed analyses of all options (cardiac myxoma, papillary fibroelastoma, rhabdomyosarcoma, and left atrial thrombus), and a neutral conclusion. The approach supports interpretable, evidence-grounded radiology question answering.

Table 2 | Accuracy of language models across zero-shot prompting, conventional online RAG, and RaR on the RadioRAG dataset

Model name	Zero-shot			Conventional online RAG			RaR	
	Accuracy (%)	Total correct (n)	*P*-value	Accuracy (%)	Total correct (n)	*P*-value	Accuracy (%)	Total correct (n)
Ministral-8B	47 ± 5 [38,57]	49	0.020	51 ± 5 [41,61]	53	0.051	66 ± 5 [57,76]	69
Mistral Large (123B)	72 ± 4 [63,81]	75	0.146	74 ± 4 [65,83]	77	0.273	81 ± 4 [72,88]	84
Llama3.3-8B	62 ± 5 [53,71]	65	0.807	63 ± 5 [55,72]	66	0.999	65 ± 5 [57,74]	68
Llama3.3-70B	76 ± 4 [67,84]	79	0.212	73 ± 4 [63,81]	76	0.081	83 ± 4 [75,89]	86
Llama3-Med42-8B	67 ± 5 [58,77]	70	0.263	67 ± 5 [59,77]	70	0.383	75 ± 4 [66,84]	78
Llama3-Med42-70B	72 ± 4 [63,80]	75	0.263	75 ± 4 [67,83]	78	0.705	79 ± 4 [71,87]	82
Llama4 Scout 16E	76 ± 4 [67,85]	79	0.392	80 ± 4 [72,88]	83	0.999	81 ± 4 [73,88]	84
DeepSeek R1-70B	78 ± 4 [70,86]	81	0.859	76 ± 4 [67,84]	79	0.662	80 ± 4 [72,88]	83
DeepSeek R1 (671B)	82 ± 4 [74,89]	85	0.859	79 ± 4 [71,87]	82	0.999	80 ± 4 [72,88]	83
DeepSeek-V3 (671B)	76 ± 4 [67,84]	79	0.106	80 ± 4 [72,88]	83	0.273	86 ± 4 [78,92]	89
Qwen 2.5-0.5B	37 ± 5 [27,46]	38	0.726	46 ± 5 [37,56]	48	0.737	42 ± 5 [32,52]	43
Qwen 2.5-3B	54 ± 5 [44,63]	56	0.146	53 ± 5 [43,62]	55	0.171	65 ± 5 [56,74]	68
Qwen 2.5-7B	55 ± 5 [45,64]	57	0.041	59 ± 5 [49,68]	61	0.171	71 ± 4 [62,80]	74
Qwen 2.5-14B	68 ± 4 [59,77]	71	0.752	67 ± 5 [57,76]	69	0.549	72 ± 4 [63,81]	75
Qwen 2.5-70B	70 ± 5 [62,79]	73	0.185	73 ± 4 [64,82]	76	0.599	78 ± 4 [70,86]	81
Qwen 3-8B	66 ± 5 [57,75]	69	0.157	73 ± 4 [65,81]	76	0.862	76 ± 4 [68,84]	79
Qwen 3-235B	82 ± 4 [74,89]	85	0.999	84 ± 4 [75,90]	87	0.999	83 ± 4 [75,89]	86
GPT-3.5-turbo	57 ± 5 [47,66]	59	0.146	62 ± 5 [53,71]	64	0.540	68 ± 5 [60,77]	71
GPT-4-turbo	76 ± 4 [67,84]	79	0.999	76 ± 4 [67,84]	79	0.999	77 ± 4 [69,85]	80
o3	86 ± 4 [78,92]	89	0.781	85 ± 4 [77,91]	88	0.705	88 ± 3 [81,93]	91
GPT-5	82 ± 4 [74,89]	85	0.097	80 ± 4 [72,88]	83	0.081	88 ± 3 [82,94]	92
MedGemma-4B-it	56 ± 5 [46,65]	58	0.157	52 ± 5 [42,62]	54	0.051	66 ± 5 [57,75]	69
MedGemma-27B-text-it	71 ± 4 [62,79]	74	0.146	75 ± 4 [66,84]	78	0.438	81 ± 4 [73,88]	84
Gemma-3-4B-it	46 ± 5 [37,56]	48	0.094	53 ± 5 [43,62]	55	0.273	62 ± 5 [52,71]	64
Gemma-3-27B-it	65 ± 5 [57,75]	68	0.157	66 ± 5 [58,75]	69	0.270	76 ± 4 [67,85]	79

Accuracy is reported in percentage as mean ± standard deviation, with 95% confidence intervals shown in brackets. Results are based on 104 questions, using bootstrapping with 1000 repetitions and replacement while preserving pairing. P-values were calculated for each model using McNemar's test on paired outcomes relative to RaR and adjusted for multiple comparisons using the false discovery rate. A $p < 0.05$ was considered statistically significant. Accuracy is presented alongside total correct answers per method.

understanding the complementary role of retrieval and reasoning. Despite already possessing clinical specialization, all four models exhibited improved diagnostic QA performance under RaR. On average, accuracy increased from 67% ± 6 under zero-shot prompting to 75% ± 6 with RaR ($P = 0.001$). Conventional online RAG, in contrast, did not show a significant improvement over zero-shot prompting (67% ± 9 vs. 67% ± 6, $P = 0.704$). Notably, RaR also significantly outperformed conventional online RAG ($P = 0.034$), suggesting that structured multi-step reasoning contributes meaningfully even when baseline knowledge is embedded through fine-tuning. Each model in this group followed a similar pattern. For instance, MedGemma-27B-text-it improved from 71% ± 4 [95% CI: 62, 79] to 81% ± 4 [95% CI: 73, 88] with RaR, MedGemma-4B-it from 56% ± 5 [95% CI: 46, 65] to 66% ± 5 [95% CI: 57, 75], Llama3-Med42-70B from 72% ± 4 [95% CI: 63, 80] to 79% ± 4 [95% CI: 71, 87], and Llama3-Med42-8B from 67% ± 5 [95% CI: 58, 77] to 75% ± 4 [95% CI: 66, 84] (see Fig. 4). While these individual gains were not statistically significant on their own, the collective improvement supports the hypothesis that retrieval-augmented reasoning provides additive benefits beyond those conferred by fine-tuning alone.

Latency and computational overhead

To evaluate the computational impact of RaR, we measured and compared per-question response times between zero-shot prompting and RaR across all models using the RadioRAG benchmark. As shown in Table 4, RaR introduced a substantial latency overhead across all model groups, with the average response time increasing from 54 ± 28 s under zero-shot prompting to 324 ± 270 s under RaR, equivalent to a 6.71× increase.

As shown in Fig. 4, this increase varied considerably by model group. Small-scale models (7–8B parameters), including Qwen 2.5-7B, Qwen3-8B, Llama3-Med42-8B, Llama3-Med42-8B, and Ministral-8B, showed a 6.04× average increase, with individual models ranging from modest (2.06× for Qwen3-8B) to substantial (35.98× for Qwen 2.5-7B). Mini models (3–4B parameters), such as Gemma-3-4B-it, MedGemma-4B-it, and Qwen 2.5-3B, exhibited the highest relative increase, averaging 11.10×, with Qwen2.5-3B peaking at 18.59×. In contrast, mid-sized models (~70B parameters), including DeepSeek-R1-70B, Llama-3.3-70B, Qwen 2.5-70B, and Llama3-Med42-70B, had a more moderate increase of 2.93×. This reflects a balance between computational capacity and the overhead introduced by iterative reasoning. For example, DeepSeek-R1-70B showed only a 1.87× increase. The large-model group (120–250B), including Qwen 3-235B, Mistral Large, and Llama4 Scout 16E, had the largest absolute latency, with a group average increase of 13.27×. Qwen3-235B showed the most pronounced jump, from 97 to 1703 s per question. Despite high computational costs, these models showed only minimal diagnostic improvement with RaR, emphasizing a potential efficiency–performance trade-off. Notably, the DeepSeek mixture of experts[52] (MoE) group (DeepSeek-R1 and DeepSeek-V3) exhibited

Table 3 | Hallucination and relevance metrics for RaR-powered responses on the RadioRAG dataset (*n* = 104)

Model name	Context relevant	Hallucination (relevant context, incorrect response)	Correct despite irrelevant context	Zero-shot incorrect → RaR correct
Ministral-8B	46% (48/104)	14% (15/104)	35% (36/104)	26% (27/104)
Mistral Large (123B)	46% (48/104)	6% (6/104)	40% (42/104)	12% (13/104)
Llama3.3-8B	46% (48/104)	17% (18/104)	37% (38/104)	12% (13/104)
Llama3.3-70B	46% (48/104)	6% (6/104)	42% (44/104)	11% (11/104)
Llama3-Med42-8B	46% (48/104)	11% (11/104)	39% (41/104)	16% (17/104)
Llama3-Med42-70B	46% (48/104)	7% (7/104)	39% (41/104)	12% (13/104)
Llama4 Scout 16E	46% (48/104)	5% (5/104)	39% (41/104)	9% (9/104)
DeepSeek R1-70B	46% (48/104)	5% (5/104)	38% (40/104)	8% (8/104)
DeepSeek R1 (671B)	46% (48/104)	3% (3/104)	37% (38/104)	6% (6/104)
DeepSeek-V3 (671B)	46% (48/104)	4% (4/104)	43% (45/104)	12% (13/104)
Qwen 2.5-0.5B	46% (48/104)	26% (27/104)	21% (22/104)	21% (22/104)
Qwen 2.5-3B	46% (48/104)	13% (14/104)	33% (34/104)	21% (22/104)
Qwen 2.5-7B	46% (48/104)	12% (12/104)	37% (38/104)	23% (24/104)
Qwen 2.5-14B	46% (48/104)	10% (10/104)	36% (37/104)	15% (16/104)
Qwen 2.5-70B	46% (48/104)	5% (5/104)	37% (38/104)	12% (13/104)
Qwen 3-8B	46% (48/104)	6% (6/104)	36% (37/104)	17% (18/104)
Qwen 3-235B	46% (48/104)	5% (5/104)	41% (43/104)	6% (6/104)
GPT-3.5-turbo	46% (48/104)	13% (14/104)	36% (37/104)	21% (22/104)
GPT-4-turbo	46% (48/104)	9% (9/104)	39% (41/104)	8% (8/104)
o3	46% (48/104)	2% (2/104)	43% (45/104)	3% (3/104)
GPT-5	46% (48/104)	3% (3/104)	45% (47/104)	7% (7/104)
MedGemma-4B-it	46% (48/104)	17% (18/104)	38% (39/104)	20% (21/104)
MedGemma-27B-text-it	46% (48/104)	3% (3/104)	38% (39/104)	15% (16/104)
Gemma-3-4B-it	46% (48/104)	20% (21/104)	36% (37/104)	25% (26/104)
Gemma-3-27B-it	46% (48/104)	7% (7/104)	37% (38/104)	20% (21/104)
Average	46% ± 0.0	*9.2% ± 6.1*	*37.4% ± 4.9*	*14.3% ± 6.5*

"Context relevant" was evaluated at the dataset level: each question was labeled as having relevant or irrelevant retrieved context, and the same label was applied across all models (48/104 questions were judged to have clinically appropriate context). "Hallucination" refers to incorrect model answers despite relevant context. "Correct despite irrelevant context" captures correct answers when the retrieved context was not clinically useful. The final column reports the percentage of questions that were incorrect in zero-shot prompting but answered correctly using RaR.

relatively efficient scaling under RaR, with an average increase of 4.19×, suggesting that sparsely activated architectures may offer runtime advantages in multi-step retrieval tasks. Similarly, the Gemma-27B group (Gemma-3-27B-it and MedGemma-27B-text-it) demonstrated a low variance and consistent response time increase of 2.82×, indicating reliable timing behavior under RaR workflow.

Despite these increases, the absolute response times remained within feasible limits for many clinical applications. Furthermore, because evaluations were conducted under identical system conditions, the relative timing metrics provide a robust measure of computational scaling. These findings suggest that while the RaR introduces additional latency, its time cost may be acceptable, especially in mid-sized and sparse-activation models depending on deployment requirements and accuracy demands.

Effect of retrieved context on human diagnostic accuracy

To better understand the source of diagnostic improvements conferred by RaR, we conducted an additional experiment involving a board-certified radiologist (T.T.N.) with seven years of experience in diagnostic and interventional radiology. As in previous evaluations, the expert first answered all 104 RadioRAG questions unaided, i.e., without access to external references or retrieval assistance, achieving an accuracy of 51% ± 5 [95% CI: 41, 62] (53/104). This baseline performance was significantly lower than that of 17 out of 25 evaluated LLMs in their zero-shot mode ($P \leq 0.017$), and not significantly different from 7 models, including GPT-3.5-turbo, Llama3.3-8B, Qwen 2.5-7B, Ministral-8B, MedGemma-4B-it, Gemma-3-4B-it, and Qwen 2.5-3B. Only Qwen 2.5-0.5B, the smallest model tested, performed significantly inferior to the radiologist (37% ± 5 [95% CI: 27, 46]; $P = 0.008$).

To isolate the contribution of retrieval independent of generative reasoning, we repeated the experiment with the same radiologist using the contextual reports retrieved by RaR, that is, the same Radiopaedia content supplied to the LLMs. With access to this structured evidence, the radiologist's accuracy increased to 68% ± 5 [95% CI: 60, 77] (71/104), a significant improvement over the unaided baseline ($P = 0.010$). This finding demonstrates that RaR successfully retrieves clinically meaningful and decision-relevant information, which can support human diagnostic accuracy even in the absence of language model synthesis.

When comparing the radiologist's context-assisted performance to that of the LLMs, only 1 out of 25 models significantly outperformed the radiologist under zero-shot conditions (o3; $P = 0.018$). In contrast, when compared to LLM performance under the full RaR framework, only 3 models, i.e., GPT-5 ($P = 0.008$), DeepSeek-V3 ($P = 0.012$) and o3 ($P = 0.008$) achieved statistically significant improvements over the context-assisted radiologist.

Generalization on an independent dataset

To assess generalizability beyond the RadioRAG benchmark, we evaluated all 25 LLMs on an independent internal dataset comprising 65 authentic radiology board examination questions from the Technical University of Munich. These questions were not included in model training or prompting

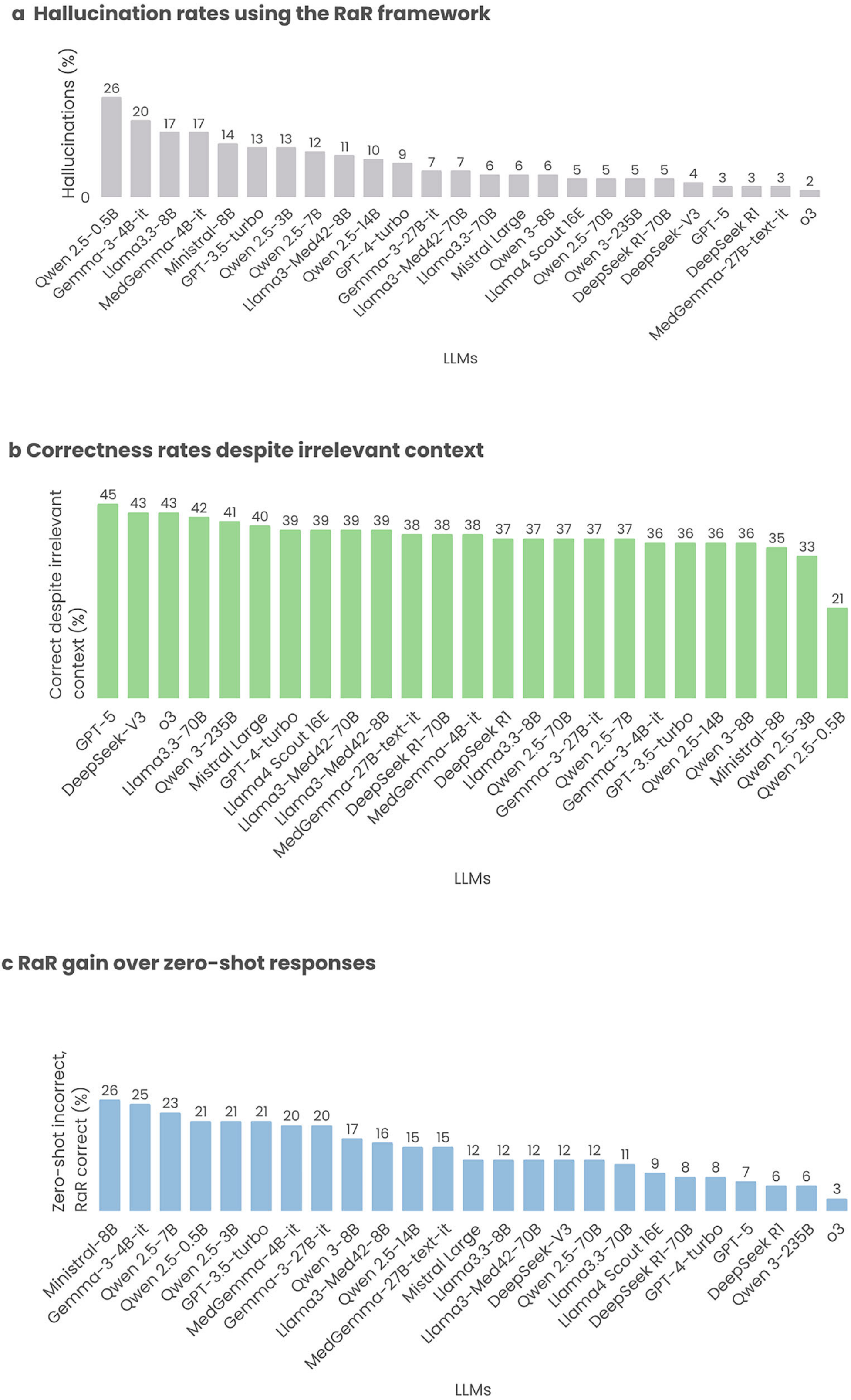

a Hallucination rates using the RaR framework

b Correctness rates despite irrelevant context

c RaR gain over zero-shot responses

Fig. 3 | Factuality assessment of LLM responses on the RadioRAG dataset. Each bar plot shows the proportion of cases per model falling into a specific factuality category, with models ordered by descending percentage. Comparisons were based on the RadioRAG benchmark dataset (n = 104).
a Hallucinations: Cases in which the provided context was relevant, but the model still generated an incorrect response (context = 1, response = 0).
b Context irrelevance tolerance: Cases where the model produced a correct response despite the retrieved context being unhelpful or irrelevant (context = 0, response = 1). **c** RaR correction: Instances where the zero-shot response was incorrect but RaR strategy successfully produced a correct response (zero-shot = 0, RaR = 1).

and reflect real-world clinical exam conditions. Results are shown in Supplementary Fig. 1. RaR again outperformed zero-shot prompting, with average accuracy increasing from 81% ± 14 to 88% ± 8 ($P = 0.002$). This replicates the overall trend observed in the main benchmark. The gain was statistically significant in small models ($P = 0.010$), but not in mid-sized ($P = 0.174$), fine-tuned ($P = 0.238$), or large models ($P = 0.953$), a contrast to the benchmark where mid-sized and fine-tuned models also showed significant improvements. This discrepancy may reflect reduced statistical power due to the smaller sample size or differences in question distribution (see Supplementary Note 4 for subgroup precision and effect size analysis).

To assess factual reliability, we replicated our hallucination analysis on the internal dataset using the same annotation protocol as in the RadioRAG

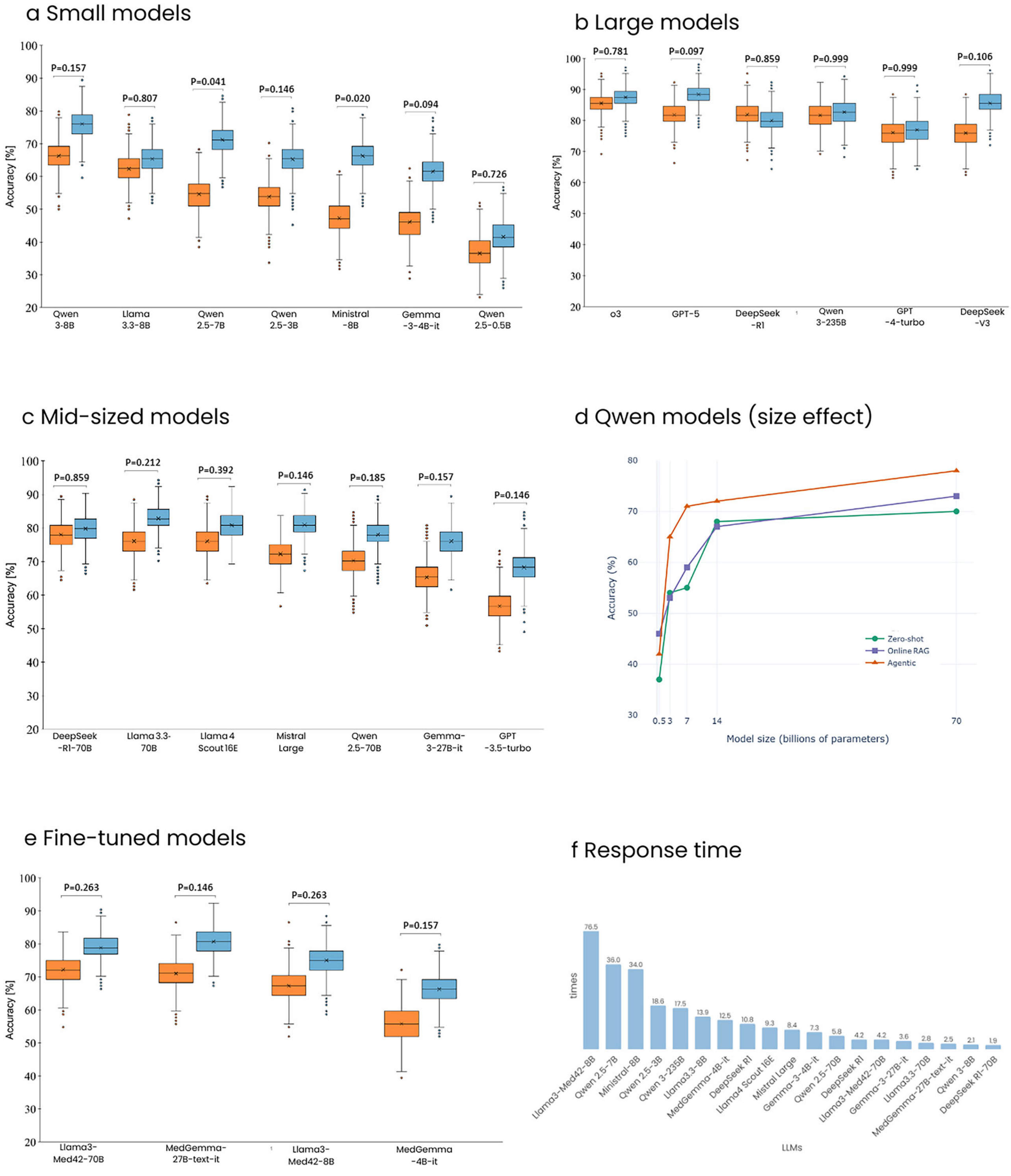

Fig. 4 | Comparative accuracy distributions and inference-time multipliers for zero-shot versus RaR strategies across model groups (RadioRAG dataset). Accuracy results are shown for **a** small-scale models (Ministral-8B, Gemma-3-4B-it, Qwen2.5-7B, Qwen2.5-3B, Qwen2.5-0.5B, Qwen3-8B, Llama3-8B), **b** large models (o3, GPT-5, DeepSeek-R1, Qwen3-235B, GPT-4-turbo, DeepSeek-V3), **c** mid-sized models (Mid-Sized Models: GPT-3.5-turbo, Llama3.3-70B, MistralLarge, Qwen2.5-70B, Llama4Scout16E, Gemma-3-27B-it, DeepSeek-R1-70B), **d** across Qwen2.5 family for different parameter sizes: Qwen2.5-70B, 14B, 7B, 3B and 0.5B, and **e** medically fine-tuned models (MedGemma27B-text-it, MedGemma4B-it, Llama3-Med42-70B, Llama3-Med42-8B). **f** Distribution of RaR-to-zero-shot runtime multipliers (× slower/faster) across all models. comparisons were performed on the RadioRAG benchmark dataset ($n = 104$). Boxplots display accuracy (%) distributions ($n = 1000$) for zero-shot (orange) and RaR (blue): boxes span Q1–Q3, central line is the median (Q2), whiskers extend to 1.5 × IQR and dots mark outliers. Line chart shows mean accuracy versus model size for zero-shot (green), onlineRAG (orange) and RaR (purple) across Qwen2.5 family. P-values were calculated between each pair's accuracy values for each model using McNemar's test on paired outcomes relative to RaR and adjusted for multiple comparisons using the false discovery rate. A $p < 0.05$ was considered statistically significant.

Table 4 | Response time comparison between zero-shot and RaR strategies on the RadioRAG dataset

Model/group name	Time			
	Zero-shot (s)	RaR (s)	Absolute difference (s)	Relative increase (times)
DeepSeek-V3 group	98.55 ± 53.58	412.7 ± 156.7	314.2 ± 141.6	4.2×
Large (120–250B) group	63.7 ± 29.4	845.1 ± 744.7	781.4 ± 715.2	13.3×
Llama4 Scout 16E	49.6 ± 24.6	462.3 ± 190.2	412.6 ± 169.7	9.3×
Mistral Large	43.9 ± 23.9	369.7 ± 142.0	325.8 ± 126.0	8.4×
Qwen 3-235B	97.5 ± 54.6	1703.3 ± 787.6	1605.8 ± 744.0	17.5×
Medium (≈ 70B) group	78.7 ± 51.4	230.58 ± 44.8	151.8 ± 34.3	2.9×
DeepSeek R1-70B	151.3 ± 83.4	282.8 ± 95.0	131.3 ± 68.3	1.9×
Llama3-Med42-70B	42.2 ± 22.4	177.0 ± 39.5	134.8 ± 27.9	4.2×
Llama3.3-70B	78.5 ± 43.6	216.7 ± 60.7	138.2 ± 34.7	2.8×
Qwen 2.5-70B	42.6 ± 22.2	245.7 ± 76.8	203.1 ± 58.5	5.8×
Gemma 27B group	75.8 ± 38.2	214.1 ± 54.9	138.3 ± 16.7	2.8×
Gemma-3-27B-it	48.8 ± 28.6	175.3 ± 37.4	126.5 ± 26.2	3.6×
MedGemma-27B-text-it	102.8 ± 56.1	253.0 ± 75.2	150.1 ± 38.4	2.5×
Small (7 – 8B) group	22.0 ± 39.9	132.9 ± 33.9	110.9 ± 9.3	6.0×
Llama3-Med42-8B	1.4 ± 0.7	108.0 ± 3.7	106.6 ± 3.3	76.5×
Llama3.3-8B	8.4 ± 4.0	116.3 ± 7.6	107.9 ± 4.6	13.9×
Ministral-8B	3.7 ± 2.2	124.9 ± 11.8	121.2 ± 10.4	34.0×
Qwen 2.5-7B	3.4 ± 1.6	122.8 ± 11.4	119.4 ± 10.4	36.0×
Qwen 3-8B	93.2 ± 53.4	192.3 ± 49.8	99.1 ± 33.9	2.1×
Mini (3 – 4B) group	11.4 ± 5.4	126.3 ± 6.3	114.9 ± 8.4	11.1×
Gemma-3-4B-it	17.5 ± 7.9	127.7 ± 13.1	110.2 ± 7.0	7.3×
MedGemma-4B-it	9.6 ± 5.4	119.4 ± 9.9	109.8 ± 9.1	12.5×
Qwen 2.5-3B	7.1 ± 3.7	131.7 ± 13.7	124.6 ± 11.0	18.6×
Average	53.7 ± 28.4	324.4 ± 270.2	271.2 ± 257.3	6.7 ± 4.1×

Average per-question response times (n = 104) are reported in seconds as mean ± standard deviation for both individual models and aggregated model groups. On the RadioRAG dataset, a fixed overhead of 10,554.6 s per model, corresponding to context generation, was evenly distributed across all questions, contributing approximately 101.5 s per question. For time analysis, models were grouped based on parameter scale and architectural characteristics into six categories: the DeepSeek mixture of experts (MoE) group, the large model group (120–250B), the medium-scale group (~70B), the Gemma-27B group, the small model group (7–8B), and the mini model group (3–4B). "Absolute difference" denotes the increase in average response time per question introduced by the RaR method, and "Relative increase" refers to the ratio of mean RaR time to mean zero-shot time per group. Statistics are computed at the group level.

benchmark. Clinically relevant evidence was retrieved in 74% (48/65) of cases, a substantial increase from the 46% observed in the main dataset. This likely reflects the more canonical phrasing and structured nature of board-style questions, which facilitate more effective document matching. Despite the higher relevance rate, hallucination rates remained consistent: the average hallucination rate, defined as incorrect answers despite clinically relevant context, was 9.2% ± 5.5%, nearly identical to the 9.2% ± 6.1 observed in the RadioRAG benchmark. Larger and reasoning-optimized models such as GPT-4-turbo (9%), DeepSeek R1 (8%), and o3 (9%) maintained their strong factual grounding, while smaller models continued to struggle, for example, Qwen 2.5-0.5B hallucinated in 32% of cases even when provided with relevant context. These results confirm that the factual consistency of RaR generalizes well across datasets, with stable hallucination behavior observed across model families. Full model-level hallucination metrics are provided in Supplementary Table 5.

To evaluate computational overhead, we repeated the time analysis on the internal dataset ($n = 65$). On the internal dataset, as shown in Supplementary Table 6, RaR inference increased average per-question response time from 35.0 ± 22.9 s under zero-shot prompting to 167.5 ± 59.4 s under RaR, an absolute increase of 132.4 ± 41.7 s, corresponding to a 6.9× ± 4.2 slowdown. These results are consistent with the RadioRAG dataset, which showed a comparable 6.7× ± 4.1 increase. Despite the smaller question set, relative latency patterns across model families remained stable: mini models (3–4B) showed the highest increase (13.7×), followed by small models (10.2×) and large models (5.9×), while mid-sized (~70B) and Gemma-27B groups demonstrated more efficient scaling (4.5× and 3.0×, respectively). The DeepSeek MoE group also maintained efficient performance (3.9×).

To benchmark human diagnostic performance on the internal dataset, we evaluated the same board-certified radiologist (T.T.N.) under two conditions: zero-shot answering and context-assisted answering using only the retrieved evidence from the RaR system. The radiologist achieved 74% ± 5 accuracy under zero-shot conditions, which increased to 85% ± 4 when supported by retrieved context, although this improvement did not reach statistical significance ($P = 0.065$). This contrasts with the main RadioRAG dataset, where context significantly boosted the radiologist's accuracy ($P = 0.010$). The diminished statistical effect in the internal dataset is likely attributable to both the higher baseline accuracy and the smaller sample size ($n = 65$), reducing the measurable headroom and statistical power, respectively. When compared directly to LLM performance, 7 out of 25 models significantly outperformed the radiologist under zero-shot prompting ($P \leq 0.014$), fewer than in the RadioRAG dataset (17/25). However, when both the human and the models were given access to the same retrieved context, no model significantly outperformed the radiologist ($P \geq 0.487$), replicating the trend observed in the main dataset (3/25).

Discussion

In this study, we introduced RaR, a radiology-specific retrieval and reasoning framework designed to enhance the performance, factual grounding, and clinical reliability of LLMs in radiology QA tasks. To the best of our knowledge, our large-scale evaluation across 25 diverse LLMs, including different architectures, parameter scales, training paradigms, and clinical fine-tuning, represents one of the most comprehensive comparative analysis of its kind to date[53]. Our findings indicate that RaR can improve diagnostic accuracy relative to conventional zero-shot prompting and conventional RAG approaches, especially in small- to mid-sized models, while also reducing hallucinated outputs. However, the benefits of RaR were not uniformly observed across all models or scenarios, underscoring the need for careful consideration of model scale and characteristics when deploying retrieval-based systems.

Beyond benchmark comparison, the originality of this work lies in demonstrating that multi-step retrieval and reasoning meaningfully enhances factual grounding and diagnostic reliability in radiology, an area where prior retrieval-augmented systems remain almost entirely single-step and unable to decompose complex clinical problems. Radiology uniquely requires hierarchical evidence integration and structured differential reasoning, yet no prior study has systematically evaluated multi-step retrieval across a large and heterogeneous cohort of state-of-the-art LLMs. By introducing a radiology-specific framework that externalizes reasoning steps, iteratively refines evidence, and operates consistently across 25 diverse models, our study establishes RaR as a new class of retrieval architecture tailored to clinical diagnostic tasks. This systematic demonstration of scalable, domain-aware multi-step retrieval represents a substantive departure from existing radiology RAG systems.

A central finding of this study is that the effectiveness of retrieval strategies strongly depends on model scale. While traditional single-step online RAG[16,18,20], and generally non-agentic RAG[16,17,54,55], approaches have previously been shown to primarily benefit smaller models (<8 billion parameters) with diminishing returns at larger scales[16,18,20], our RaR framework expanded performance improvements into the mid-sized model range (approximately 17–150 billion parameters). Mid-sized models such as GPT-3.5-turbo, Mistral Large, and Llama3.3-70B have sufficient reasoning capabilities to follow structured logic but frequently struggle to independently identify and incorporate relevant external clinical evidence. By decomposing complex clinical questions into structured subtasks and iteratively retrieving targeted evidence, RaR consistently improved accuracy across these mid-sized models, gains that conventional RAG did not achieve in this important segment. Similarly, smaller models also benefited from structured retrieval, overcoming some limitations associated with fewer parameters and less comprehensive pretraining. However, the magnitude of improvements varied between individual small-scale models, likely reflecting differences in architectural design, instruction tuning, and pretraining data. These results suggest that while RaR can broadly enhance performance across smaller and mid-sized models, model-specific optimizations may be required to fully capitalize on its potential.

In contrast, the largest evaluated models (more than 200 billion parameters), such as GPT-5, o3, DeepSeek-R1, and Qwen-3-235B, exhibited minimal to no gains from either conventional or RaR methods. These models achieved high performance with zero-shot inference alone, suggesting that their extensive pretraining on large-scale and potentially clinically relevant data already equipped them with substantial internal knowledge. Beyond pretraining coverage, additional factors likely contribute to this saturation effect. Very large models are known to possess advanced reasoning capabilities, robust in-context learning, and architectural enhancements such as deeper transformer stacks or mixture-of-experts routing, which collectively reduce reliance on external retrieval. These mechanisms may allow large models to internally simulate multi-step reasoning without explicit retrieval augmentation. While retrieval therefore offered limited incremental accuracy benefits at this scale, it may still provide value in clinical practice by enhancing transparency, auditability, and alignment with established documentation standards. Future studies should explore whether RaR can improve interpretability, consistency, and traceability of decisions made by these high-capacity models, even when raw accuracy does not substantially increase.

To further examine the relationship between model scale and retrieval benefit, we conducted a controlled scaling analysis using the Qwen 2.5 model family. This approach, which held architecture and training constant, revealed a strong positive relationship between model size and diagnostic accuracy across all tested inference strategies[56,57]. Nevertheless, the optimal retrieval approach varied: traditional single-step RAG offered the greatest advantage for smaller models, whereas RaR consistently enhanced mid-sized model performance. These results highlight the importance of aligning retrieval strategies with the intrinsic reasoning capacity of individual models, emphasizing tailored rather than universal implementation of retrieval augmentation.

A key consideration in clinical applications is whether domain-specific fine-tuning reduces the necessity or utility of external retrieval. Clinically specialized LLMs, such as variants of MedGemma and Llama3-Med42, are often assumed to contain embedded medical knowledge sufficient for diagnostic reasoning[6]. However, our results show that even these fine-tuned models consistently benefited from RaR: across all four tested models, performance significantly improved when structured evidence was introduced. Nevertheless, fine-tuning itself did not consistently improve diagnostic accuracy compared to general-domain counterparts of similar scale. For example, Llama3-Med42-70B underperformed relative to the non-specialized Llama3.3-70B, despite its radiology-specific adaptation. This finding lends support to concerns that fine-tuning, especially when not carefully balanced, may introduce trade-offs such as catastrophic forgetting or reduced general reasoning ability. Taken together, our results suggest that RaR remains essential even in specialized models, and that domain-specific fine-tuning should not be assumed to universally enhance performance. Instead, retrieval and fine-tuning may offer partially complementary benefits, but their interaction appears model- and implementation-dependent, warranting further empirical scrutiny.

These findings also carry practical implications for model selection. For institutions with limited computational resources, RaR enables smaller and mid-sized models to achieve diagnostic accuracy closer to that of much larger systems, making them a cost-effective option. Very large models (>200B) deliver high baseline accuracy without retrieval, but their marginal benefit from RaR is limited, suggesting they may be more appropriate in settings where resources and latency are less constrained. Clinically fine-tuned models, meanwhile, continue to benefit from RaR, highlighting that retrieval should be viewed as complementary rather than optional. Thus, the optimal choice of model depends on balancing accuracy needs, interpretability, and resource constraints within the intended clinical context.

Beyond accuracy, our analysis demonstrated that RaR improved factual grounding[6,14] and reduced hallucinations in model outputs. By systematically associating diagnostic responses with specific retrieved content from Radiopaedia.org[19], the framework promoted evidence-based reasoning, which is critical in safety-sensitive applications like radiology. Although clinically relevant evidence was retrieved in less than half of the evaluated cases, most models successfully leveraged this content to produce factually correct responses when it was available. Larger and clinically tuned models demonstrated robustness by correctly responding even when retrieved evidence was irrelevant or insufficient, likely relying on internal knowledge[15]. However, such internally derived answers, while accurate, lack explicit grounding in external sources, raising potential concerns for interpretability and clinical accountability[58]. Smaller models were less resilient when retrieval failed, highlighting their greater reliance on structured external support. Consequently, ensuring high-quality retrieval remains paramount, especially for deployment scenarios where transparency and traceability of decisions are required.

Another noteworthy finding is the relatively frequent occurrence of correct answers despite irrelevant retrieved context. This behavior most likely reflects strong prior knowledge and reasoning capacity in larger and reasoning-optimized models, which can generate accurate responses even when the retrieved evidence is noisy or clinically unhelpful. At the same time, it also indicates retrieval noise or mismatched document selection, where the pipeline surfaces content that is adjacent but not clinically useful.

On the one hand, this resilience highlights the capacity of well-trained LLMs to integrate internal knowledge with limited external support[59], a desirable feature when retrieval systems fail. On the other hand, it raises important considerations for interpretability and accountability[60]: correct answers derived without external grounding may be less transparent, harder to audit, and more difficult for clinicians to trust in safety-critical settings. To illustrate this duality, we provide representative examples in Supplementary Note 2 where models answered correctly despite irrelevant or misleading retrieved excerpts, with annotations showing whether the correctness likely stemmed from internal knowledge or partial overlap with the question. These cases emphasize that retrieval systems play a dual role—not only supplying missing information but also providing traceable evidence that clinicians can verify. Future work should therefore focus on disentangling knowledge-driven versus retrieval-driven correctness, minimizing retrieval noise, and designing systems that can explicitly indicate whether an answer is primarily evidence-grounded or internally derived.

The increased diagnostic reliability introduced by RaR came at a computational cost. Response times significantly increased compared to zero-shot inference due to iterative query refinement, structured evidence gathering, and multi-step coordination. This latency varied substantially by model size and architecture, with smaller models experiencing the largest relative increases, and mid-sized or sparsely activated architectures demonstrating comparatively moderate overhead. Very large models, although capable of achieving high accuracy without retrieval, experienced substantial absolute latency increases without commensurate accuracy gains. Future work should therefore explore optimization strategies to manage computational overhead, such as selective retrieval triggering, parallel evidence pipelines, or methods to distill reasoning into more efficient inference paths.

A related concern is the potential for self-preference bias, since o3 contributed to distractor generation and GPT-4o-mini was used as the orchestration controller in RaR. We emphasize that distractor generation and benchmarking were conducted through fully separated pipelines, and all distractors were systematically reviewed by a board-certified radiologist before inclusion, ensuring that final multiple-choice questions were clinically valid and unbiased. GPT-4o-mini was not evaluated as a question-answering model and played no role in dataset construction or adjudication. Moreover, the multiple-choice framework with human-curated distractors and purely accuracy-based scoring substantially mitigates the risk of self-preference bias, which is more relevant in style-sensitive or evaluator-graded tasks. All models, including those from the GPT family, received identical finalized inputs, and thus operated under the same information constraints. Indeed, recent work suggests that in fact-centric benchmarks with verifiable answers, self-preference effects diminish substantially or align with genuine model superiority[61]. Nevertheless, we acknowledge that future studies could strengthen methodological rigor by ensuring complete model-family independence in dataset construction and orchestration components.

Furthermore, RaR demonstrated value as a decision-support tool for human experts. Providing a board-certified radiologist with the same retrieved context as the RaR system substantially improved their diagnostic accuracy compared to unaided performance. This finding illustrates that the RaR process successfully identified and presented clinically meaningful, decision-relevant evidence that directly supported expert reasoning. The limited number of LLMs significantly outperforming the context-assisted radiologist further underscores the complementary strengths of human expertise and retrieved information. Thus, RaR may serve dual purposes in clinical environments, simultaneously enhancing LLM performance and providing interpretable, actionable evidence to clinicians. These findings highlight that RaR is not merely a benchmarking improvement but a clinically relevant mechanism for structuring and externalizing reasoning, enabling radiologists to verify evidence, interpret model logic, and incorporate AI-derived context directly into diagnostic workflows.

To evaluate whether our findings generalize beyond the RadioRAG benchmark setting, we replicated our analysis on an unseen dataset of radiology board examination questions from a different institution. RaR again improved diagnostic accuracy over zero-shot prompting, preserved factual consistency, and reduced hallucination rates across models, confirming its robustness across settings. However, not all trends reproduced fully. Improvements for mid-sized and clinically fine-tuned models were no longer statistically significant, and the gain from RaR context for the human expert did not reach significance. These discrepancies likely stem from two factors: the smaller sample size of the internal dataset, which reduced statistical power, and the more structured phrasing of board-style questions, which may have facilitated stronger baseline performance for both humans and models. In particular, the higher relevance rate of retrieved evidence in this dataset suggests that the more canonical language of exam-style questions enabled better document matching, narrowing the performance gap between zero-shot and RaR conditions. These findings underscore that while the benefits of RaR broadly generalize, their magnitude may depend on dataset-specific features such as question format and baseline difficulty.

Our study has several important limitations. First, our evaluation relied exclusively on Radiopaedia.org, a trusted, peer-reviewed, and openly accessible radiology knowledge source. We selected Radiopaedia to ensure high-quality and clinically validated content, and we secured explicit approval for its use in this study. While other resources exist, many are either not openly accessible, not peer-reviewed in full, or require separate agreements that were not feasible within the scope of this work. Dependence on a single data provider, however, may restrict retrieval coverage and not capture the full breadth of radiological knowledge. Future studies should aim to incorporate additional authoritative sources, structured knowledge bases, or clinical ontologies to improve coverage and generalizability. Second, although our evaluation spanned two datasets, i.e., (i) the public RadioRAG benchmark (n = 104) and (ii) an independent board-style dataset from the Technical University of Munich (n = 65), the total number of questions remains relatively modest. While both datasets are expert-curated and clinically grounded, larger and more diverse collections encompassing broader clinical scenarios, imaging modalities, and diagnostic challenges are needed to fully assess the robustness and generalizability of RaR. Expanded datasets would also enable higher-powered subgroup analyses and stronger statistical certainty for model- and task-level comparisons. However, creating radiology QA items is highly resource-intensive, requiring significant time and multiple rounds of board-certified radiologist review to ensure that questions are text-based, clinically meaningful, and free from data leakage. To help address this gap, we publicly release our newly developed internal dataset alongside this manuscript, thereby contributing to cumulative dataset growth and enabling future research. Third, the RaR process incurs significant computational overhead, substantially increasing response times compared to conventional zero-shot prompting and traditional single-step RAG. Although response durations remained within feasible limits for non-emergent clinical use cases, the practicality of the proposed method in time-sensitive settings (e.g., acute diagnostic workflows) remains uncertain. Future research should explore optimization techniques, such as parallelization or selective module activation, to mitigate latency without sacrificing diagnostic accuracy or reasoning quality. Fourth, both the RadioRAG and internal board-style datasets consist of static, retrospective QA items that, while clinically representative, do not fully capture the complexity and dynamism of real-world radiology practice. Clinical workflows often involve multimodal inputs (e.g., imaging data, clinical reports), evolving case presentations, and dynamic clinician-AI interactions, none of which are modeled in benchmark-style question formats. Importantly, our study was limited to text-only QA. The multiple-choice format was introduced solely as a benchmarking tool to enable reproducible accuracy measurement across models and humans; in real-world settings, RaR is intended to support open-ended, text-based clinical questions (e.g., “what is the most likely diagnosis given these findings?”) rather than exam-style queries. While this design strengthens internal validity, it restricts direct applicability to multimodal radiology tasks. As such, our findings reflect performance in controlled QA environments rather than in prospective or embedded clinical contexts. Future research should therefore validate RaR in real clinical systems, ideally in prospective studies embedded within reporting workflows or decision-support platforms, to assess practical utility, safety, and user impact under real-world conditions. Fifth, despite evaluating a broad range of LLM architectures, parameter scales, and training paradigms, we observed substantial variability in the diagnostic gains attributable to RaR across individual models. This likely reflects a combination of factors, including architectural differences, instruction tuning approaches, and pretraining data composition, as well as implementation-specific elements such as prompt design and module orchestration. Because the RaR pipeline relies on structured prompting and task decomposition, its performance may be sensitive to changes in phrasing, retrieval heuristics, or module coordination. Future work should systematically investigate both model-level and implementation-level sources of variability to develop more robust, generalizable retrieval strategies tailored to different model configurations. Sixth, although the framework improved diagnostic accuracy and factual reliability, it introduced substantial latency overhead. While response durations remained within feasible ranges for non-emergent settings, future research should explore optimization strategies such as asynchronous retrieval, selective triggering of agentic reasoning when model uncertainty is high, and more efficient orchestration of multi-agent pipelines to balance accuracy with computational efficiency. Finally, although accuracy was scored using a constrained LLM adjudicator, we manually validated the procedure by reviewing 100 model-response pairs (5 models × 20 questions) and found complete agreement with the automated labels. Future implementations could further improve reproducibility by enforcing structured outputs (e.g., a JSON field specifying the selected option) to enable deterministic letter-matching without requiring an adjudicator model.

This study presents a proof-of-concept for a multi-step retrieval and reasoning framework capable of enhancing diagnostic accuracy, factual reliability, and clinical interpretability of LLMs in radiology QA tasks. Our extensive, large-scale analysis of 25 diverse models highlights the complex relationships between retrieval strategy, model scale, and clinical fine-tuning. While RaR shows clear promise, particularly for mid-sized and clinically optimized models, future research is essential to refine retrieval mechanisms, mitigate computational overhead, and validate these systems across broader clinical contexts. As generative AI continues to integrate into medical practice, frameworks emphasizing transparency, evidence-based reasoning, and human-aligned interpretability, such as the RaR approach introduced here, will become increasingly critical for trustworthy and effective clinical decision support. Beyond serving as an automated reasoning pipeline, RaR may also provide a foundation for human–AI collaborative diagnosis. By structuring and externalizing evidence synthesis, the framework enables clinicians to review, validate, and integrate retrieved knowledge into their own diagnostic reasoning. Future iterations of RaR should therefore be explicitly designed to support collaborative workflows, where AI augments rather than replaces clinical expertise, ultimately improving diagnostic confidence, accountability, and patient safety.

Methods

Ethics statement

The methods were performed in accordance with relevant guidelines and regulations. The data utilized in this research was sourced from previously published studies. As the study did not involve human subjects or patients, it was exempt from institutional review board approval and did not require informed consent.

Dataset

This study utilized two carefully curated datasets specifically designed to evaluate the performance of RaR-powered LLMs in retrieval-augmented radiology QA.

As our primary dataset, we utilized two previously published datasets from the RadioRAG study[18]: the RSNA-RadioQA[18] and ExtendedQA[18] datasets. The RSNA-RadioQA dataset consists of 80 radiology questions derived from peer-reviewed cases available in the Radiological Society of North America (RSNA) Case Collection. This dataset covers 18 radiologic subspecialties, including breast imaging, chest radiology, gastrointestinal imaging, musculoskeletal imaging, neuroradiology, and pediatric radiology, among others. Each subspecialty contains at least five questions, carefully crafted from clinical histories and imaging descriptions provided in the original RSNA case documentation. Differential diagnoses explicitly listed by original case authors were excluded to avoid biasing model responses. Images were intentionally excluded. Detailed characteristics, including patient demographics and subspecialty distributions, have been previously published and are publicly accessible. The ExtendedQA dataset consists of 24 unique, radiology-specific questions initially developed and validated by board-certified radiologists with substantial diagnostic radiology experience (5–14 years). These questions reflect realistic clinical diagnostic scenarios not previously available online or included in known LLM training datasets. The final RadioRAG dataset used in this study subsequently contains 104 questions combining both RSNA-RadioQA and ExtendedQA.

To ensure consistent evaluation across all models and inference strategies, we applied structured preprocessing to the original RadioRAG dataset, particularly the ExtendedQA portion ($n = 24$), which was initially formatted as open-ended questions. All questions from the RSNA-RadioQA dataset ($n = 80$) were left unchanged. However, for the ExtendedQA subset, each question was first converted into a multiple-choice format while preserving the original stem and correct answer. To standardize the evaluation across both RSNA-RadioQA and ExtendedQA, we then generated three high-quality distractor options for every question in the dataset ($n = 104$), resulting in a total of four answer choices per item. Distractors were generated using OpenAI's GPT-4o and o3 models, selected for their ability to produce clinically plausible and contextually challenging alternatives. Prompts were designed to elicit difficult distractors, including common misconceptions, closely related entities, or synonyms of the correct answer. All distractors were subsequently reviewed in a structured process by a board-certified radiologist to confirm that they were clinically meaningful, non-trivial, and free of misleading or implausible content. Items failing this review were discarded or revised until they met expert standards. Although o3 and GPT-4o were used to generate preliminary distractors, these were only intermediate drafts. All final multiple-choice options were curated and approved through expert review, ensuring that benchmark items were clinically meaningful, unbiased, and identical across all models irrespective of origin. This hybrid pipeline of LLM-assisted distractor generation plus systematic expert validation has precedent in the educational technology and medical education literature, where it has been shown to produce valid and challenging MCQs when coupled with human oversight[62]. A representative prompt used for distractor generation was:

> *"I have a dataset of radiology questions that are currently open-ended, each with a correct answer provided. I want to transform these into multiple-choice questions (MCQs) by generating four answer options per question (one correct answer + three distractors). The distractors should be plausible and the level of difficulty must be high. If possible, include distractors that are synonyms, closely related concepts, or common misconceptions related to the correct answer."*

Supplementary Table 1 summarizes the characteristics of the RadioRAG dataset used in this study. The original RSNA-RadioQA questions are publicly available through their original publication[18].

In addition to the publicly available RadioRAG dataset, we constructed an internal dataset of 65 radiology questions to further evaluate model performance on knowledge domains aligned with German board certification requirements. This dataset was developed and validated by board-certified radiologists (L.A. with 9 and K.B. 10 years of clinical experience across subspecialties). Questions were derived from representative diagnostic cases and key concepts covered in the German radiology training curriculum at the Technical University of Munich, ensuring coverage of essential knowledge expected of practicing radiologists in Germany. None of the questions or their formulations are available in online case collections or known LLM training corpora.

The internal dataset was formatted as multiple-choice questions following the same pipeline as ExtendedQA. Each question contains 5 options. The dataset is publicly available for research purposes in Supplementary Note 5.

Experimental design

All retrieval in this study was performed using Radiopaedia.org, a peer-reviewed and openly accessible radiology knowledge base. Radiopaedia was chosen to ensure high-quality and clinically validated content, minimizing the risk of unverified or non-peer-reviewed material. While other authoritative databases exist, many are either not openly available, lack consistent peer review, or require access agreements that were not feasible within the scope of this work. For Radiopaedia, explicit approval for research use was obtained prior to conducting this study.

The experimental design centers on an orchestrated retrieval and reasoning framework adapted from LangChain's Open Deep Research pipeline, specifically tailored for radiology QA tasks. As illustrated in Fig. 1, the pipeline employs a structured, multi-step workflow designed to produce comprehensive, evidence-based diagnostic reports for each multiple-choice question. The reasoning and content-generation process within the RaR orchestration is powered by OpenAI's GPT-4o-mini model, selected for its proficiency in complex reasoning tasks, robust instruction-following, and effective tool utilization. The architecture consists of two specialized modules: (i) a supervisor module and (ii) a research module, coordinated through a stateful directed graph framework. State management within this directed graph framework ensures that all steps in the workflow remain consistent and coordinated. The system maintains a shared memory state, recording the research plan, retrieved evidence, completed drafts, and all module interactions, enabling structured progression from planning through final synthesis. Importantly, GPT-4o-mini functioned only as a fixed orchestration engine coordinating retrieval and structuring evidence; the final diagnostic answer (i.e., the selected option) was always generated by the target model under evaluation. This ensures comparability across models but also clarifies that RaR evaluates how models use structured retrieved evidence rather than their independent ability to perform multi-step reasoning. Because the orchestration process and retrieved context were identical across all tested models, including GPT-family systems, GPT-4o-mini's involvement did not confer any preferential advantage; all models operated under the same inputs and conditions.

To enable structured, multi-step reasoning in the RaR framework, we implemented a preprocessing step focused on diagnostic abstraction. For each question in the RadioRAG dataset, we used the Mistral Large model to generate a concise, comma-separated summary of key clinical concepts. We selected Mistral Large after preliminary comparisons with alternative LLMs (e.g., GPT-4o-mini, LLaMA-2-70B), as it consistently produced concise, clinically faithful keyword summaries with minimal redundancy, making it particularly well-suited for guiding retrieval (see Supplementary Note 1 for representative examples). This step was designed to extract the essential diagnostic elements of each question while filtering out rhetorical structure, instructional phrasing (e.g., "What is the most likely diagnosis?"), and other non-clinical language. These keyword summaries served exclusively as internal inputs to guide the RaR system's retrieval process and were not shown to the LLMs as part of the actual question content. The intent was to ensure retrieval was driven by the clinical essence of the question rather than superficial linguistic cues. The prompt used for keyword extraction was:

"*Extract and summarize the key clinical details from the following radiology question. Provide a concise, comma-separated summary of keywords and key phrases in one sentence only.*

Question: {question_text}.

Summary:"

The workflow is coordinated primarily by two modules, each with distinct responsibilities: (i) supervisor module and (ii) research module. The supervisor acts as the central orchestrator of the pipeline. Upon receiving a question, the supervisor reviews the diagnostic keywords and multiple-choice options, then formulates a structured research plan dividing the task into clearly defined sections, one for each diagnostic option. This module assigns tasks to individual research modules, each responsible for exploring a single diagnostic choice. Throughout the process, the supervisor ensures strict neutrality, focusing solely on evidence gathering rather than advocating for any particular option. After research modules complete their tasks, the supervisor synthesizes their outputs into a final report, utilizing specialized tools to generate an objective introduction and conclusion.

Each research module independently conducts an in-depth analysis focused on one diagnostic option. Beginning with a clear directive from the supervisor, the research module employs a structured retrieval strategy to obtain relevant evidence. This involves an initial focused query using only essential terms from the diagnostic option, followed by contextual queries combining these terms with clinical features from the question stem (e.g., imaging findings or patient demographics). If retrieval results are inadequate, the module adaptively refines queries by simplifying terms or substituting synonyms. In cases where sufficient evidence is not available after four attempts, the module explicitly documents this limitation. All retrieval tasks utilize Radiopaedia.org exclusively, ensuring clinical accuracy and reliability. After completing retrieval, the research module synthesizes findings into a structured report segment, explicitly highlighting both supporting and contradicting evidence. Each segment includes clearly formatted citations linking directly to source materials, ensuring transparency and verifiability.

To facilitate structured retrieval and writing processes, the pipeline utilizes a suite of specialized computational tools dynamically selected based on specific task requirements: (i) search tool, (ii) report structuring tools, and (iii) content generation tool. In the following, details of each tool is explained.

The retrieval mechanism is powered by a custom-built search tool leveraging a locally hosted instance of SearXNG, a privacy-oriented metasearch engine deployed within a containerized Docker environment. This setup ensures consistent and reproducible search results. To maintain quality and clinical reliability, the search tool restricts results exclusively to content from Radiopaedia.org through a two-layer filtering process: first by appending a "site:radiopaedia.org" clause to all queries, and subsequently by performing an explicit domain check on all retrieved results. Raw results are deduplicated and formatted into markdown bundles suitable for seamless integration into subsequent reasoning steps.

The supervisor module employs specific tools to structure the diagnostic report systematically. An initial Sections tool is used to outline the report into distinct diagnostic sections, aligning precisely with the multiple-choice options. Additional specialized tools generate standardized Introduction and Conclusion sections: the Introduction tool summarizes essential clinical details from the question, and the Conclusion tool objectively synthesizes findings from all diagnostic sections, emphasizing comparative diagnostic considerations without bias.

The research module utilizes a dedicated Section writing tool to construct standardized report segments. Each segment begins with a concise synthesis of retrieved evidence, followed by interpretive summaries clearly identifying points supporting and contradicting each diagnostic choice. Citations are integrated inline, referencing specific Radiopaedia[19] URLs for traceability.

Upon completion of individual research segments, the supervisor module compiles the final diagnostic report, verifying the completeness and quality of all sections. The resulting structured report, including introduction, detailed analysis of diagnostic options, and conclusion, is then immediately persisted in a robust manner. Reports are streamed incrementally into newline-delimited JSON (NDJSON) format, preventing data loss in case of interruptions. This storage method supports efficient resumption by checking previously completed entries, thus avoiding redundant processing. After processing all questions within a given batch, individual NDJSON entries are consolidated into a single comprehensive JSON file, facilitating downstream analysis and evaluation.

Baseline comparison systems

Each model was evaluated under three configurations: (i) zero-shot prompting (conventional QA), (ii) conventional online RAG[18], and (iii) our proposed RaR framework.

In the zero-shot prompting baseline, models received no external retrieval assistance or context. Instead, each model was presented solely with the multiple-choice questions from the RadioRAG dataset (question stem and four diagnostic options) and prompted to select the correct answer based entirely on their pre-trained knowledge. Models generated their responses autonomously without iterative feedback, reasoning prompts, or additional information.

The exact standardized prompt used for this configuration is provided below:

> *"You are a highly knowledgeable medical expert. Below is a multiple-choice radiology question. Read the question carefully. Provide the correct answer by selecting the most appropriate option from A, B, C, or D.*
>
> *Question:*
>
> *{question}*
>
> *Options:*
>
> *{options}"*

The conventional online RAG baseline was implemented following a state-of-the-art non-agentic retrieval framework previously developed for radiology question answering by Tayebi Arasteh et al.[18]. The system employs GPT-3.5-turbo to automatically extract up to five representative radiology keywords from each question, optimized experimentally to balance retrieval quality and efficiency. These keywords were used to retrieve relevant articles from Radiopaedia.org, with each article segmented into overlapping chunks of 1000 tokens. Chunks were then converted into vector embeddings (OpenAI's text-embedding-ada-002) and stored in a temporary vector database. Subsequently, the embedded original question was compared against this database to retrieve the top three matching text chunks based on cosine similarity. These retrieved chunks served as external context provided to each LLM alongside the original multiple-choice question. Models were then instructed to answer concisely based solely on this context, explicitly stating if the answer was unknown.

The exact standardized prompt used for this configuration is provided below:

> *"You are a highly knowledgeable medical expert. Below is a multiple-choice radiology question accompanied by relevant context (report). First, read the report, and then the question carefully. Use the retrieved context to answer the question by selecting the most appropriate option from A, B, C, or D. Otherwise, if you don't know the answer, just say that you don't know.*
>
> *Report:*
>
> *{report}*
>
> *Question:*
>
> *{question}*
>
> *Options:*
>
> *{options}"*

Evaluation

S.W., J.S., T.T.N., and S.T.A. performed model evaluations. We assessed both small and large-scale LLMs using responses generated between July 1 and August 22, 2025. For each of the 104 questions in the RadioRAG benchmark dataset, as well as each of the 65 questions in the unseen generalization dataset, models were integrated into a unified evaluation pipeline to ensure consistent testing conditions across all settings. The evaluation included 25 LLMs: Ministral-8B, Mistral Large, Llama3.3-8B[45,46], Llama3.3-70B[45,46], Llama3-Med42-8B[43], Llama3-Med42-70B[43], Llama4 Scout 16E[33], DeepSeek R1-70B[44], DeepSeek-R1[44], DeepSeek-V3[47], Qwen 2.5-0.5B[41], Qwen 2.5-3B[41], Qwen 2.5-7B[41], Qwen 2.5-14B[41], Qwen 2.5-70B[41], Qwen 3-8B[48], Qwen 3-235B[48], GPT-3.5-turbo, GPT-4-turbo[8], o3, GPT-5[49], MedGemma-4B-it[42], MedGemma-27B-text-it[42], Gemma-3-4B-it[50,51], and Gemma-3-27B-it[50,51]. These models span a broad range of parameter scales (from 0.5B to over 670B), training paradigms (instruction-tuned, reasoning-optimized, clinically aligned, and general-purpose), and access models (open-source, open-weights, or proprietary). They also reflect architectural diversity, including dense transformers and MoE[52] systems. Full model specifications, including size, category, accessibility, knowledge cutoff date, context length, and developer are provided in Table 1. For clarity, GPT-5 is included here as a widely used system-level benchmark. As noted in OpenAI's documentation, GPT-5 internally routes queries across different underlying models depending on the task, and should therefore be regarded as a system rather than a fixed architecture. All models were run with deterministic decoding parameters (temperature = 0, top-p = 1, no top-k or nucleus sampling). No random seeds or stochastic ensembles were used, and each model produced a single, reproducible response per question. This ensured that performance differences reflected model reasoning ability rather than variability introduced by random sampling.

Accuracy was determined by comparing each LLM's response to the correct option. For this, we used Mistral Large as an automated adjudicator. Importantly, this role was not generative reasoning but a constrained verification task: the adjudicator only needed to check whether the correct option appeared in the response. This made the process essentially binary option-matching rather than open-ended judgment, thereby minimizing any risk of hallucination.

Constrained decoding was not applied during answer generation; instead, each model was explicitly prompted to select one option (A–D for the RadioRAG benchmark, or A–E for the internal dataset). In rare cases where a model output included multiple options (e.g., "A and D"), scoring was based strictly on whether the correct option appeared explicitly and unambiguously in the response. If the correct option was included, the response was counted as correct; otherwise, it was scored as incorrect. This ensured reproducibility and avoided bias across models.

For each multiple-choice question, both the LLM's response and the correct answer (including its corresponding letter and option) were provided to Mistral Large via a standardized prompt. The adjudicator was explicitly instructed to respond only with "Yes" if the correct answer was present, or "No" otherwise, ensuring that outputs were strictly bounded and reproducible. A "Yes" was scored as 1 (correct), and a "No" was scored as 0 (incorrect), ensuring a consistent and unbiased measure of diagnostic accuracy.

The exact standardized prompt used for this configuration is provided below:

> *"You are a highly knowledgeable medical expert. Determine whether the Correct Answer appears within the LLMs response, fully or as a clear part of the explanation, even if the wording differs. Respond with 'Yes' if the Correct Answer can be found in the LLMs response; otherwise respond with 'No'.*
>
> *LLMs response:*
>
> *{llms_response}*
>
> *Correct Answer:*
>
> *{correct_answer}"*

To validate this automated procedure, we manually reviewed 20 questions for 5 representative LLMs spanning different model families and parameter scales (DeepSeek-R1, o3, Llama3.3-70B, MedGemma-27B-text-it, and Qwen 2.5-3B), corresponding to 100 model-response pairs. In this sample, manual inspection showed complete concordance with the adjudicator's Yes/No labels, and no discrepancies were identified.

To evaluate the factual reliability of model outputs under the RaR framework, we conducted a targeted hallucination analysis across all 104 questions in the RadioRAG benchmark[18] (and separately across all 65 questions in the unseen generalization dataset). This analysis aimed to differentiate model errors due to flawed reasoning from those caused by insufficient or irrelevant evidence, and to assess the extent to which final answers were grounded in the retrieved context. Each RaR response was reviewed by a board-certified radiologist (T.T.N.) with seven years of experience in diagnostic and interventional radiology. For every question, the following three criteria were assessed: (i) whether the retrieved Radiopaedia context was clinically relevant to the question, (ii) whether the model's final answer was consistent with that context, and (iii) whether the final answer was factually correct. Context was classified as clinically relevant only if it contained no incorrect or off-topic content with respect to the diagnostic question. This strict definition ensured that relevance was not based on superficial keyword overlap but on the actual clinical utility of the content. Retrievals were deemed relevant only when the retrieved material included appropriate imaging findings, clinical clues, or differential diagnoses applicable to the question stem. Hallucinations were defined as cases in which the model produced an incorrect answer despite being provided with clinically relevant context. These represent failures of reasoning or synthesis rather than of retrieval. Given the high-stakes nature of radiologic diagnosis, identifying such errors is essential for understanding model reliability and safety. We also documented instances where models answered questions correctly despite being supplied with irrelevant or unhelpful context. These "correct despite irrelevant context" cases reflect scenarios in which the model relied on internal knowledge rather than external grounding. While not classified as hallucinations, these responses raise questions about the transparency, traceability, and consistency of model behavior in the absence of meaningful retrieval.

To evaluate the computational cost associated with RaR, we measured per-question response times for both zero-shot prompting and the RaR framework using the 104-question RadioRAG benchmark (and separately using the 65 questions of the unseen generalization dataset). Timing logs were collected from structured output directories for each model. For each dataset, we measured a fixed initialization overhead corresponding to the context construction phase unique to RaR inference. On the RadioRAG dataset ($n = 104$), this overhead averaged 10,554.6 s per model (≈101.5 s per question). On the internal dataset ($n = 65$), the overhead averaged 5754.9 s per model (≈88.5 s per question). Together, this corresponds to a total of 16,301 s across both datasets, or ≈97 s per question on average. These overheads were distributed uniformly across all questions to ensure fair per-question latency estimates. To ensure robust comparison and mitigate the influence of extreme values, outlier durations were handled using the Tukey method[63]. Specifically, any response time that exceeded the typical upper range, defined as values greater than the third quartile by more than 1.5 times the interquartile range, was considered an outlier and replaced with the mean of the remaining non-outlier values for that model and inference strategy. For each model, we computed the mean and standard deviation of response times under both conditions. Additionally, we calculated the absolute difference in average response time per question and the relative increase, defined as the ratio of mean RaR response time to mean zero-shot response time. To contextualize timing behavior across a heterogeneous model set, we grouped models according to both parameter scale and architectural characteristics. This grouping approach reflected the practical computational load of each model more accurately than parameter count alone. Six distinct groups were defined: (i) the DeepSeek MoE group, including DeepSeek-R1 and DeepSeek-V3; (ii) the large model group (120–250 billion parameters), including Qwen 3-235B, Mistral Large, and Llama4 Scout 16E; (iii) the medium-scale group (~70B), comprising DeepSeek R1-70B, Llama3.3-70B, Qwen2.5-70B, and Llama3-Med42-70B; (iv) the Gemma-27B group, containing Gemma-3-27B-it and MedGemma-27B-text-it; (v) the small model group (7–8B), including Qwen 2.5-70B, Qwen3-8B, Llama3-Med42-8B, Llama3.3-8B, and Ministral-8B; and (vi) the mini model group (3–4B), consisting of Gemma-3-4B-it, MedGemma-4B-it, and Qwen 2.5-3B. Group-level averages and standard deviations were calculated across constituent models and are reported in Table 4. All timing evaluations were performed under identical system conditions to ensure fair comparisons. While absolute response times may vary with hardware and load, the relative increases provide a stable and interpretable metric for assessing the computational implications of RaR.

To benchmark LLM performance against domain expertise, we conducted a human evaluation involving a board-certified radiologist (T.T.N.) with seven years of experience in diagnostic and interventional radiology. The evaluation followed a two-phase design to mirror the LLM configurations. In the first phase, the radiologist answered all 104 questions from the RadioRAG benchmark (and separately all 65 questions from the internal generalization dataset) without any external assistance, analogous to zero-shot prompting. The expert was fully blinded to the LLM responses, dataset construction process, and reference standard answers, which remained inaccessible throughout the entire study, including after task completion and up to manuscript submission. Responses were recorded as final, and no additional time or information resources were permitted during this phase. In the second phase, we aimed to isolate the contribution of the RaR component, independent of generative reasoning. For this, the same radiologist was provided with the contextual evidence retrieved by the RaR system for each question, the same Radiopaedia excerpts that were used as inputs for RaR-powered LLM inference. The radiologist completed this phase only after finishing the unaided zero-shot phase, and did not have access to the correct answers or to their own previous responses, thereby avoiding bias from prior knowledge. The radiologist answered the same 104 questions again (and separately the same 65 questions of the internal generalization dataset), this time using the retrieved context as decision support, without access to the original question-answer pairs or their previous responses. The format and presentation of the contextual evidence were identical to what the LLMs received during RaR-powered inference, ensuring comparability. This design enabled us to disentangle the effects of information retrieval from language model reasoning, by comparing unaided radiologist performance, radiologist performance with context, and RaR-based LLM outputs under standardized conditions. Accuracy was computed using the same evaluation criteria applied to LLMs. Statistical comparisons between human and model responses were performed using McNemar's test on paired question-level outcomes. Confidence intervals and p-values were adjusted for multiple comparisons using the false discovery rate.

Statistical analysis

Statistical analysis was performed using Python v3.11 with SciPy v1.10, NumPy v1.25.2, and statsmodels v0.14.5 packages. For each dataset, bootstrapping with 1,000 redraws was used to estimate means, standard deviations, and 95% confidence intervals (CI)[64]. A strictly paired design ensured identical redraws across conditions[65]. To assess statistical significance of individual model-level comparisons between inference strategies, exact McNemar's test[66] (based on the binomial distribution) was applied to each model separately on paired question-level outcomes. Resulting p-values were corrected for multiple comparisons using the false discovery rate, with a significance threshold of 0.05. These values are reported in Table 2 and per-model Results subsections. For group-level comparisons (e.g., zero-shot vs. RaR across mid-sized models), paired two-tailed t-tests were used to compare average accuracy across all models in the group. These p-values therefore reflect differences at the cohort level rather than for any single model, and are explicitly labeled as such in the Results. To explore the relationship between model size and performance, Pearson correlation coefficients were computed between parameter counts and accuracy values within the Qwen 2.5 model family, separately for each inference strategy.

Data availability

All data in this study are available. The RadioRAG dataset including the original RSNA-RadioQA and ExtendedQA are available via the original RadioRAG publication. The new unseen internal dataset is available in Supplementary Note 5.

Code availability

All source code, configurations, and parameters used in this work are publicly available. The RaR pipeline, developed in Python 3.11, is available at: https://github.com/sopajeta/RaR. Our implementation relies on several key frameworks and tools. We used LangChain Open Deep Research (https://github.com/langchain-ai/deep-research) for experimental modules, LangChain v0.3.25 (https://github.com/langchain-ai/langchain) for orchestration and management, and LangGraph v0.4.1 (https://github.com/langchain-ai/langgraph) to support multi-step control flow and task decomposition. Model access and embedding generation were handled via the OpenAI Python SDK v1.77.0 (https://platform.openai.com). The SearxNG metasearch engine (https://github.com/searxng/searxng) was also deployed via Docker v25.0.2 (https://www.docker.com) and used for online web retrieval. The traditional online RAG pipeline is hosted at https://github.com/tayebiarasteh/RadioRAG, which relies on the LangChain v0.1.0, Chroma (https://www.trychroma.com) for vector storage, and the OpenAI API v1.12 for embeddings. All locally deployed language models sourced from Hugging Face, were assessed and used between July 1 – August 22, 2025, and are explicitly listed below, with corresponding URLs: Qwen2.5-0.5B: https://huggingface.co/Qwen/Qwen2.5-0.5B. Qwen2.5-3B: https://huggingface.co/Qwen/Qwen2.5-3B. Qwen2.5-7B: https://huggingface.co/Qwen/Qwen2.5-7B. Qwen2.5-14B: https://huggingface.co/Qwen/Qwen2.5-14B. Qwen 2.5-70B: https://huggingface.co/Qwen/Qwen2.5-72B. Qwen 3-8B: https://huggingface.co/Qwen/Qwen3-8B. Qwen 3-235B: https://huggingface.co/Qwen/Qwen3-235B-A22B. Llama3.3-8B: https://huggingface.co/meta-llama/Meta-Llama-3-8B. Llama3.3-70B: https://huggingface.co/meta-llama/Llama-3.3-70B-Instruct. Llama 3-Med42-70B: https://huggingface.co/m42-health/Llama3-Med42-70B. Llama 3-Med42-8B: https://huggingface.co/m42-health/Llama3-Med42-8B. Llama4 Scout 16E: https://huggingface.co/meta-llama/Llama-4-Scout-17B-16E. Mistral Large: https://huggingface.co/mistralai/Mistral-Large-Instruct-2407. Ministral8B: https://huggingface.co/mistralai/Ministral-8B-Instruct-2410. Gemma-3-4B-it: https://huggingface.co/google/gemma-3-4b-it. Gemma-3-27B-it: https://huggingface.co/google/gemma-3-27b-it. Medgemma-4B-it: https://huggingface.co/google/medgemma-4b-it. Medgemma-27B-text-it: https://huggingface.co/google/medgemma-27b-text-it. DeepSeek-V3: https://huggingface.co/deepseek-ai/DeepSeek-V3. DeepSeek-R1: https://huggingface.co/deepseek-ai/DeepSeek-R1. DeepSeek-R1-70B: https://huggingface.co/deepseek-ai/DeepSeek-R1-Distill-Llama-70B. All the previously mentioned LLMs were served using vLLM v0.9.0 (https://github.com/vllm-project/vllm) with tensor parallelism set to the number of GPUs inside the node, except for models under 3 billion parameters, which were served without tensor parallelism. All OpenAI-hosted models were accessed through direct REST API calls to the OpenAI endpoints (https://platform.openai.com). The exact versions employed in this study are as follows:. GPT-5 (2025-08-07). O3 (2025-04-16). GPT-4-Turbo (2024-04-09). GPT-3.5-Turbo (2024-01-25). For the majority of experiments, particularly those involving standard LLMs, the computations were performed on GPU nodes equipped with Nvidia H100 and H200 accelerators. The H100 configuration consisted of four Nvidia H100 GPUs, each providing 94 GB of HBM2e memory and operating at a 500 W power limit. These GPUs were paired with two AMD EPYC 9554 "Genoa" processors based on the Zen 4 architecture, each offering 64 high-performance cores running at 3.1 GHz. The H200 configuration featured four Nvidia H200 GPUs, each offering 141 GB of high-bandwidth memory also at 500 W, coupled to the same dual AMD EPYC 9554 processor configuration. This combination of high-end Nvidia accelerators from NHR@FAU's Helma Cluster (https://doc.nhr.fau.de/clusters/helma/) provided the necessary computational capabilities for inferencing the majority of the LLMs used during our experiments. Experiments involving extremely large-scale architectures, such as the DeepSeek R1 or V3 model and other similarly demanding workloads, were executed on nodes equipped with AMD's MI300-series accelerators. In these cases, the MI300X configuration was utilized, which combined a dual-socket AMD EPYC 9474 F platform with a total of 96 CPU cores and 2304 GB of DDR5-5600 system memory, together with eight AMD Instinct MI300X accelerators. Each MI300X GPU offered 192 GB of memory, enabling inference runs that required massive parameter counts and exceptional memory capacity (Deepseek R1 with 671 billion parameters). Additional experimentation also leveraged AMD Instinct MI300A nodes that integrate 24-core CPUs with unified on-package memory, with a total of 512 GB shared across four accelerators. The hardware used in our experiments included a local machine with an Intel Pentium CPU with 2 cores and 8 GB Memory for consuming API endpoints.

Received: 24 August 2025; Accepted: 4 December 2025;
Published online: 22 December 2025

References

1. Akinci D'Antonoli, T. et al. Large language models in radiology: fundamentals, applications, ethical considerations, risks, and future directions. *Diagn. Interv. Radiol.* https://doi.org/10.4274/dir.2023.232417 (2023).
2. Buess, L., Keicher, M., Navab, N., Maier, A. & Tayebi Arasteh, S. From large language models to multimodal AI: a scoping review on the potential of generative AI in medicine. *Biomed. Eng. Lett*. **15**, 1–19 (2025).
3. Tayebi Arasteh, S. et al. The treasure trove hidden in plain sight: the utility of GPT-4 in chest radiograph evaluation. *Radiology* **313**, e233441 (2024).
4. Clusmann, J. et al. The future landscape of large language models in medicine. *Commun. Med.* **3**, 141 (2023).
5. Thirunavukarasu, A. J. et al. Large language models in medicine. *Nat. Med.* **29**, 1930–1940 (2023).
6. Singhal, K. et al. Large language models encode clinical knowledge. *Nature* **620**, 172–180 (2023).
7. Arora, A. & Arora, A. The promise of large language models in health care. *Lancet* **401**, 641 (2023).
8. OpenAI. GPT-4 Technical Report. Preprint at http://arxiv.org/abs/2303.08774 (2023).
9. Fink, M. A. et al. Potential of ChatGPT and GPT-4 for data mining of free-text CT reports on lung cancer. *Radiology* **308**, e231362 (2023).
10. Adams, L. C. et al. Leveraging GPT-4 for post hoc transformation of free-text radiology reports into structured reporting: a multilingual feasibility study. *Radiology* **307**, e230725 (2023).

11. Kottlors, J. et al. Feasibility of differential diagnosis based on imaging patterns using a large language model. *Radiology* **308**, e231167 (2023).
12. Schmidt, R. A. et al. Generative large language models for detection of speech recognition errors in radiology reports. *Radiol. Artif. Intell.* **6**, e230205 (2024).
13. Lewis, P. et al. Retrieval-Augmented generation for knowledge-intensive NLP Tasks. in *Adv. Neural Inform. Proces. Sys.* (eds. Larochelle, H., Ranzato, M., Hadsell, R., Balcan, M. F. & Lin, H.) **33**, 9459–9474 (Curran Associates, Inc., 2020).
14. Alkaissi, H. & McFarlane, S. I. Artificial Hallucinations in ChatGPT: implications in scientific writing. *Cureus* **15**, e35179 (2023).
15. Ji, Z. et al. Survey of Hallucination in Natural Language Generation. *ACM Comput. Surv.* **55**, 1–38 (2023).
16. Zakka, C. et al. Almanac—retrieval-augmented language models for clinical medicine. *NEJM AI* **1**, (2024).
17. Xiong, G., Jin, Q., Lu, Z. & Zhang, A. Benchmarking retrieval-augmented generation for medicine. In *Findings of the Association for Computational Linguistics: ACL 2024,* (eds Ku, L-W., Martins, A. & Srikumar, V.) 6233–6251 (Association for Computational Linguistics, Bangkok, Thailand, 2024).
18. Tayebi Arasteh, S. et al. RadioRAG: online retrieval–augmented generation for radiology question answering. *Radiol. Artif. Intell.* **7**, e240476 (2025).
19. Radiopaedia Australia Pty Ltd ACN 133 562 722. Radiopaedia https://radiopaedia.org/.
20. Fink, A., Rau, A., Reisert, M., Bamberg, F. & Russe, M. F. Retrieval-augmented generation with large language models in radiology: from theory to practice. *Radiol. Artif. Intell.* **7**, e240790 (2025).
21. Brown, T. B. et al. Language models are few-shot learners. in *Proc. 34th International Conference on Neural Information Processing Systems.* **159**, 1877–1901 (2020).
22. Tayebi Arasteh, S. et al. Large language models streamline automated machine learning for clinical studies. *Nat. Commun.* **15**, 1603 (2024).
23. Ferber, D. et al. Development and validation of an autonomous artificial intelligence agent for clinical decision-making in oncology. *Nat. Cancer* https://doi.org/10.1038/s43018-025-00991-6 (2025).
24. Wang, L. et al. A survey on large language model based autonomous agents. *Front. Comput. Sci*. **18**, 186345 (2024).
25. Xiong, G. et al. Improving Retrieval-augmented generation in medicine with iterative follow-up questions. In *Biocomputing 2025: Proceedings of the Pacific Symposium*, Vol. 30, 199–214 (2024).
26. Yang, D. et al. MedAide: information fusion and anatomy of medical intents via LLM-based agent collaboration. *Inform. Fusion* **127**, 103743 (2026).
27. Jiang, Y. et al. MedAgentBench: a virtual EHR environment to benchmark medical LLM agents. *NEJM AI* **2**, AIdbp2500144 (2025).
28. Liu, J. et al. Medchain: Bridging the Gap Between LLM agents and clinical practice through interactive sequential benchmarking. Preprint at https://doi.org/10.48550/arXiv.2412.01605 (2024).
29. Mao, Y., Xu, W., Qin, Y. & Gao, Y. CT-Agent: a multimodal-LLM agent for 3D CT radiology question answering. Preprint at https://doi.org/10.48550/arXiv.2505.16229 (2025).
30. Zeng, F., Lyu, Z., Li, Q. & Li, X. Enhancing LLMs for Impression Generation in Radiology Reports through a Multi-Agent System. Preprint at https://doi.org/10.48550/arXiv.2412.06828 (2024).
31. Yi, Z., Xiao, T. & Albert, M. V. A Multimodal Multi-Agent Framework for Radiology Report Generation. Preprint at https://doi.org/10.48550/arXiv.2505.09787 (2025).
32. Ben-Atya, H. et al. Agent-based uncertainty awareness improves automated radiology report labeling with an open-source large language model. Preprint at https://doi.org/10.48550/arXiv.2502.01691 (2025).
33. Zhou, H.-Y. et al. MedVersa: a generalist foundation model for medical image interpretation. Preprint at https://doi.org/10.48550/ARXIV.2405.07988 (2024).
34. Schick, T. et al. Toolformer: language models can teach themselves to use tools. *Adv. Neural Inform. Process. Syst.* **36**, 68539–68551 (2023).
35. Yao, S. et al. React: synergizing reasoning and acting in language models. In *International Conference on Learning Representations (ICLR)* (ICLR, Kigali, Rwanda, 2023).
36. Truhn, D., Reis-Filho, J. S. & Kather, J. N. Large language models should be used as scientific reasoning engines, not knowledge databases. *Nat. Med.* **29**, 2983–2984 (2023).
37. Wei, J. et al. Chain-of-thought prompting elicits reasoning in large language models. *Adv. Neural Inform. Process. Syst.* **35**, 24824–24837 (2022).
38. Karunanayake, N. Next-generation agentic AI for transforming healthcare. *Inform. Health* **2**, 73–83 (2025).
39. Khattab, O. et al. Dspy: Compiling declarative language model calls into self-improving pipelines. Poster in Workshop: Workshop on robustness of zero/few-shot learning in foundation models (R0-FoMo) https://neurips.cc/virtual/2023/76693 (2023).
40. Koçak, B. & Meşe, İ. AI agents in radiology: toward autonomous and adaptive intelligence. *dir* https://doi.org/10.4274/dir.2025.253470 (2025).
41. Bai, J. et al. Qwen technical report. Preprint at https://doi.org/10.48550/arXiv.2309.16609 (2023).
42. Sellergren, A. et al. MedGemma Technical Report. Preprint at https://doi.org/10.48550/arXiv.2507.05201 (2025).
43. Christophe, C., Kanithi, P. K., Raha, T., Khan, S. & Pimentel, M. A. Med42-v2: a suite of clinical LLMs. Preprint at https://doi.org/10.48550/arXiv.2408.06142 (2024).
44. Guo, D. et al. DeepSeek-R1 incentivizes reasoning in LLMs through reinforcement learning. *Nature* **645**, 633–638 (2025).
45. Touvron, H. et al. LLaMA: open and efficient foundation language models. Preprint at http://arxiv.org/abs/2302.13971 (2023).
46. Grattafiori, A.et al. The Llama 3 herd of models. Preprint at https://doi.org/10.48550/arXiv.2407.21783 (2024).
47. Liu, A. et al. Deepseek-v3 technical report. Preprint at https://doi.org/10.48550/arXiv.2412.19437 (2024).
48. Yang, A. et al. Qwen3 technical report. Preprint at https://doi.org/10.48550/arXiv.2505.09388 (2025).
49. OpenAI. Introducing GPT-5. https://openai.com/index/introducing-gpt-5/ (2025).
50. Team, G. et al. Gemma: Open models based on gemini research and technology. Preprint at https://doi.org/10.48550/arXiv.2403.08295 (2024).
51. Team, G. et al. Gemma 3 technical report. Preprint at https://doi.org/10.48550/arXiv.2503.19786 (2025).
52. Jacobs, R. A., Jordan, M. I., Nowlan, S. J. & Hinton, G. E. Adaptive mixtures of local experts. *Neural Comput.* **3**, 79–87 (1991).
53. Bakhshandeh, S. Benchmarking medical large language models. *Nat. Rev. Bioeng.* **1**, 543–543 (2023).
54. Wang, C. et al. Potential for GPT technology to optimize future clinical decision-making using retrieval-augmented generation. *Ann. Biomed. Eng.* **52**, 1115–1118 (2024).
55. Kresevic, S. et al. Optimization of hepatological clinical guidelines interpretation by large language models: a retrieval augmented generation-based framework. *npj Digit. Med.* **7**, 102 (2024).
56. Hoffmann, J. et al. Training compute-optimal large language models. *NIPS'22: Proc. 36th International Conference on Neural Information Processing Systems,* 30016–30030 (Curran Associates Inc., 2022).
57. Kaplan, J. et al. Scaling laws for neural language models. Preprint at https://doi.org/10.48550/arXiv.2001.08361 (2020).
58. Gilbert, S., Kather, J. N. & Hogan, A. Augmented non-hallucinating large language models as medical information curators. *npj Digit. Med.* **7**, 100 (2024).
59. Ren, R. et al. Investigating the factual knowledge boundary of large language models with retrieval augmentation. In *Proc. 31st International Conference on Computational Linguistics,* 3697–3715 (Association for Computational Linguistics, 2025).

60. Chen, H., Gomez, C., Huang, C.-M. & Unberath, M. Explainable medical imaging AI needs human-centered design: guidelines and evidence from a systematic review. *npj Digit. Med.* **5**, 156 (2022).
61. Chen, Y.-S., Jin, J., Kuo, P.-T., Huang, C.-W. & Chen, Y.-N. LLMs are Biased Evaluators But Not Biased for Fact-Centric Retrieval Augmented Generation. In *Findings of the Association for Computational Linguistics: ACL 2025,* (eds Che, W., Nabende, J., Shutova, E. & Pilehvar, M. T.) 26669–26684 (Association for Computational Linguistics, Vienna, Austria, 2025).
62. Grévisse, C., Pavlou, M. A. S. & Schneider, J. G. Docimological quality analysis of LLM-Generated multiple choice questions in computer science and medicine. *SN Comput. Sci.* **5**, 636 (2024).
63. Tukey, J. W. *Exploratory Data Analysis* (Springer, 1977).
64. Konietschke, F. & Pauly, M. Bootstrapping and permuting paired t-test type statistics. *Stat. Comput.* **24**, 283–296 (2014).
65. Khader, F. et al. Artificial intelligence for clinical interpretation of bedside chest radiographs. *Radiology* **307**, e220510 (2022).
66. McNemar, Q. Note on the sampling error of the difference between correlated proportions or percentages. *Psychometrika* **12**, 153–157 (1947).

Acknowledgements

This research is supported by BayernKI, the central infrastructure for the State of Bavaria to advance academic AI research. The authors gratefully acknowledge the HPC resources provided by the Erlangen National High Performance Computing Center (NHR@FAU) of the Friedrich-Alexander-Universität Erlangen-Nürnberg. NHR funding is provided by federal and Bavarian state authorities. NHR@FAU hardware is partially funded by the Deutsche Forschungsgemeinschaft (DFG) – 440719683. D.T. was supported by grants from the DFG (NE 2136/3-1, LI3893/6-1, TR 1700/7-1) and is supported by the German Federal Ministry of Education (TRANSFORM LIVER, 031L0312A; SWAG, 01KD2215B) and the European Union's Horizon Europe and innovation programme (ODELIA [Open Consortium for Decentralized Medical Artificial Intelligence], 101057091). K.B. received grants from the European Union (101079894), Bayern Innovativ, German Federal Ministry of Education and Research, Max Kade Foundation, and Wilhelm-Sander Foundation.

Author contributions

The formal analysis was conducted by S.W., J.S., and S.T.A. The original draft was written by S.T.A., J.S., and S.W. and edited by S.T.A. J.S. developed the codes for analysis and pipeline; S.W. configured and maintained the LLM-serving infrastructure. The experiments were performed by S.W. and J.S. The statistical analyses were performed by S.W., J.S., and S.T.A. The internal dataset was curated by L.A. and K.B. D.T., T.T.N., K.B., L.A., M.R., and S.T.A. provided clinical expertise. S.W., J.S., D.T., M.L., T.T.N., K.B., M.R., H.K., G.W., A.M., and S.T.A. provided technical expertise. The study was defined by S.T.A. All authors read the manuscript and agreed to the submission of this paper.

Funding

Open Access funding enabled and organized by Projekt DEAL.

Competing interests

S.W. is partially employed by DATEV eG, Germany. D.T. received honoraria for lectures by Bayer, G.E., Roche, AstraZeneca, and Philips and holds shares in StratifAI GmbH, Germany, and in Synagen GmbH, Germany. M.L. is employed by Generali Deutschland Services GmbH, Germany and is an editorial board at European Radiology Experimental. K.B. and L.A. are trainee editorial boards at Radiology: Artificial Intelligence. A.M. is an associate editor at IEEE Transactions on Medical Imaging. S.T.A. is an editorial board at Communications Medicine and at European Radiology Experimental, a trainee editorial board at Radiology: Artificial Intelligence, and was partially employed by Synagen GmbH, Germany. The other authors do not have any competing interests to disclose.

Additional information

Supplementary information The online version contains supplementary material available at https://doi.org/10.1038/s41746-025-02250-5.

Correspondence and requests for materials should be addressed to Soroosh Tayebi Arasteh.

Reprints and permissions information is available at http://www.nature.com/reprints